Literature study

Feasibility of Solar Thermal Propulsion

A. Takken
4212118

Delft University of Technology

TU Delft Delft University of Technology

Challenge the future

Image taken from https://www.permanent.com/space-transportation-steam-rockets.html [1].

Contents

Preface

This literature study report is part of the project which is to be undertaken at Delft University of Technology (DUT). It encompasses the practical study towards the subject of Solar Thermal Propulsion (STP). This report is preceded by a project proposal [2], stating the background of STP research and the outline of this document. The literature study itself, which lies in front of you, shows thoroughly what research was done in the last decades and what can be done to advance the application of STP on (nano)satellites. The literature study will be accompanied by a new proposal, which will describe the actions that will be undertaken for the final thesis.

There is still plenty of work left to do in the coming months at DUT. For now, I would like to thank my supervisor ir. Zandbergen, who helped me out when I was stuck and who was a continuous support for me. Furthermore, special thanks go out to my fellow students in the master room on the 8th floor here, who are always a source of inspiration and (occasionally) laughter.

Following this, I will be working on the thesis, in order to conclude my master's degree at the faculty of Faculty of Aerospace Engineering (AE) at DUT. I am looking forward to it.

A. Takken, 4212118
Delft, July 2019

List of Figures

List of Tables

Acronyms

3mE	Faculty of Mechanical, Maritime and Materials Engineering
AE	Faculty of Aerospace Engineering
AFRPL	Air Force Rocket Propulsion Laboratory
DAO	Design, Analysis and Optimization
DAQ	Data Acquisition
DUT	Delft University of Technology
GEO	Geostationary Earth Orbit
HEEO	Highly Elliptical Earth Orbit
IRT	Ideal Rocket Theory
ISUS	Integrated Solar Upper Stage
LabVIEW	Laboratory Virtual Instrument Engineering Workbench
LEO	Low Earth Orbit
MEMS	Microelectromechanical Systems
MLI	Multi-Layer Insulation
NASA	National Aeronautics and Space Administration
NI	National Instruments
NIST	National Institute of Standards and Technology
ORC	Organic Rankine Cycle
RAC	Receiver-Absorber Cavity
SL	Sea Level
SOTV	Solar Orbit Transfer Vehicle
STP	Solar Thermal Propulsion
STT1	Solar Thermal Thruster 1
STT2	Solar Thermal Thruster 2
TNW	Faculty of Applied Physics
TRL	Technology Readiness Level
TRP	Thermal Rocket Propulsion

List of symbols

Latin

B	Blow down ratio
C_d	Discharge coefficient
D	Diameter
F	Thrust
I_{sp}	Specific impulse
K	Shell-to-tank factor
L	Length
MM	Molar mass
M_t	Throat Mach number
$Mass$	Mass
P_{in}	Input power
R	Specific gas constant
R_A	Universal gas constant
Re	Reynolds number
R	Shell radius
$T0$	Temperature at inner side of the RAC inner wall
$T1$	Temperature at outer side of the RAC inner wall
$T2$	Temperature at inner side of the RAC outer wall
$T3$	Temperature at outer side of the RAC outer wall
T_c	Propellant chamber temperature
T_p	Propellant temperature
T	Temperature
c_p	Specific heat coefficient
c^*	Characteristic velocity
f	Moody friction factor
h_α	Coefficient of convective heat transfer
j	Safety factor
m	Number of channels
n	Number of elements
p_a	Ambient pressure
p_e	Exit pressure
q	Heat flux
t	Thickness
v	Velocity

Greek

ΔV	DeltaV
Γ	Vandenkerckhove function
α	Absorption
ϵ	Emissivity
γ	Specific heat ratio
μ_t	Throat dynamic viscosity
μ	Dynamic viscosity
ρ	Density
σ	Stefan-Boltzmann constant
σ	Yield stress

Subscripts

c	chamber
f	final
g	pressurant gas
i	initial
l	loss
p	propellant
t	throat
t	tank

Abstract

In this report, one will find a literature study which focuses on the concept of STP. STP revolves around the heating of a propellant through (focused) solar radiation. The goal of the project, which this report is part of, is to demonstrate the feasibility of a solar thermal thruster for nanosatellite applications. The pathway will be to design, manufacture and test this thruster in order to validate the predicted performance and assess whether the concept is feasible.

Before that path will be taken, research is documented and reviewed in this document. The advantages, disadvantage and hurdles that are associated with STP are described. Next to that, a tool is introduced, called the STP tool, predicting the motor performance in terms of thrust and specific impulse. This tool will be used to design the motor. This motor is then subject to experiments, of which the data will be compared to the tool output, in order to confirm the feasibility of STP. Please note that the proposal for the final thesis is documented in the proposal which is concurrent to this document. Furthermore, it was found out if it is actually possible to conduct high-powered experiments at DUT. It was concluded that it is, due to light source and equipment availability. Unfortunately, it remains to be seen how the manufacturability will go and how it will impact the design process.

In the concluding chapter, a rough outline for the thesis, based on this document, was given:

1. Extend the performance tool, especially regarding view factors. These enhancements will be based on the work Preijde did in his thesis [10].
2. Design the Solar Thermal Thruster 2 (STT2) using the knowledge gained from this literature study. This is closely concurrent with the next step, being the manufacturing, and the tool developed before to reach optimum performance. It is no use to design a motor which cannot be made within the resources provided.
3. Manufacture STT2. This will be done within the environment of DUT and, as said before, closely related to the design step.
4. Predict motor performance, including specific impulse (I_{sp}), thrust, temperature and pressure.
5. Setup experiments.
6. Conduct experiments.
7. Analyse data.
8. Conclude on the feasibility of STP and provide recommendations.

After the proposal document is constructed, work will thus commence on extending the performance tool with view factors, after which the actual designing of the engine will be done.

1

Introduction

In the past decade, the increase of nanosatellites has been undeniably large (see Figure 1.1 [3]). According to the figure, it is expected to rise in the coming years as well. Nanosatellites, of which CubeSats and PocketQubes are examples [2], are reliant on propulsion subsystems to function. One of the concepts developed for this subsystem is STP.

STP hinges on the idea of heating a propellant through (focused) solar radiation without any form of combustion. It boasts high specific impulse (in the range of 800-1000 s) combined with average thrust levels (up to 1 N) [11]. This positions the concept between chemical and electric propulsion as a promising concept for e.g. Earth orbit maneuvers which need to be done in matters of days with high efficiency [12, 13].

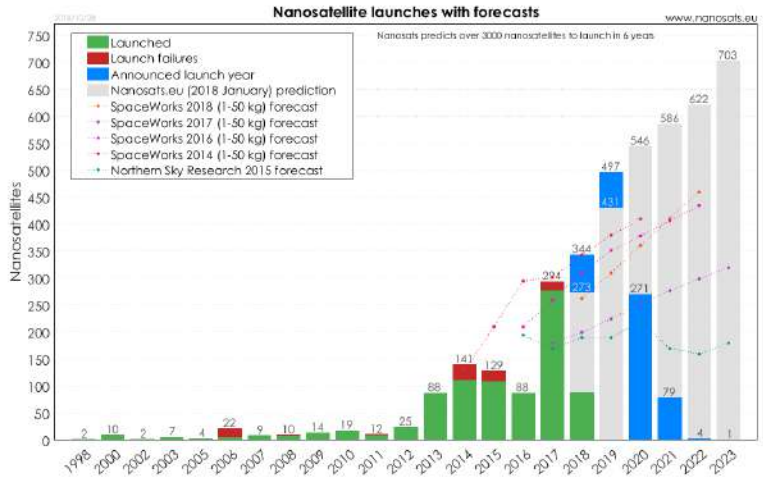

Figure 1.1: Nanosatellite launches and forecast [3].

STP is currently still under development, without having been flown in space [11]. This can largely be explained by the fact that it requires an excessive amount of investment into the concentrator system, which has to be built from scratch [14]. Next to that, the required solar illumination also imposed challenges due to eclipses and attitude control. These latter challenges can be mitigated by using thermal storage units and fiber optic cables, but they add to the complexity of the system [15]. All in all, multiple studies were undertaken towards STP, but the Technology Readiness Level (TRL) still rests at level 3 [16], about which more in Chapter 2. This level implies that the next step should be to conduct laboratory-based studies towards validation.

Based on this, it is decided to look into practical studies, or tests, for STP. Because of the limitations in resources (think about time, money and facilities), the experiments should be kept simple. Testing a motor under illumination, without concentrator system and heat storage unit to keep the complexity at a minimum, would be a way to assess whether the performance (medium thrust, high efficiency or specific impulse) associated with STP [17] [11].

To carry out these experiments, first research into the subject of STP needs to be found and assessed. That is where this document comes in, the literature study. It serves as a means to find out what needs to be done to develop STP into a full-grown propulsion option for (nano)spacecraft applications.

Now that the goal of the report has been stated, the lay-out will be handed to the reader. The document will kick off with Chapter 2 describing first what STP is, followed by its components. Then the history of research is thoroughly given, with a dedicated section on research done at DUT. In the end, a section on Leenders' work, similar to the work that will be carried out for this project, is shown. The chapter closes off with a critical assessment on the research, distilling what is most important for this project.

Chapter 3 describes the tool developed to assess components of an STP thruster. It consists of three distinctive sections: the feed system tool, the Receiver-Absorber Cavity (RAC) tool and the nozzle & performance tool. They are all combined in a Python script, which can be found in Appendix A. They incorporate literature and output a model that is to be used to predict the final performance of the to-be-developed motor. For validation, the experiments are needed.

These experiments, or how to acquire data from it, are described in Chapter 4. It shows the search for a suitable light source, followed by the equipment and software needed to conduct the tests. Furthermore, a test plan was written which is presented in Appendix B.

In the end, conclusions will be drawn regarding the chapters described above. Furthermore, recommendations will be given to further improve the literature study report.

2

Research

This chapter will show the state of the art of STP and (previous) research conducted towards the topic. A portion of what will be presented has already been described in the project plan made for this thesis [2].

The chapter is divided into five parts: first, the concept of STP and its components are shown, followed by the history and research of STP nowadays. Then, research into STP at DUT is presented, followed by a critical assessment of the research studied. Finally, a layout of Leenders' thesis [6], a precursor of this study, is described and discussed.

2.1. Concept & components

STP is a propulsion concept developed for the field of space travel. The idea encompasses the use of solar irradiance to heat a propellant without converting the solar energy into electrical energy. The heated propellant is then expelled via a nozzle to create thrust. To increase the efficiency of the system, multiple (parabolic) mirrors and lenses are often used [18–20].

STP is a promising concept, as it brings a boost in specific impulse when compared to conventional chemical propulsion, enabling the designer to have a lighter spacecraft (when keeping the payload mass at the same level) or increasing the payload mass without increasing the total spacecraft mass [11, 21]. In Figure 2.1, a schematic of an STP system is shown [4].

STP delivers, in theory, a higher specific impulse than conventional liquid thrusters. According to Leverone et al. [11], mono-propellant and bi-propellant thrusters are listed at 150-320 s, while STP concepts reach 203-860 s. A higher specific impulse implies a lower total system mass and/or a higher payload mass, which could decrease the cost of launching a satellite equipped with STP significantly. Electric propulsion, such as Hall effect thrusters and ion engines, has an even higher I_{sp} (up to 5930 s), but is limited by its thrust (maximum of 50 mN) in comparison to STP [11, 22]. Thrust in turn determines the amount of time needed for a manoeuvre or orbit transfer. Thus, STP is more efficient than (liquid) chemical thrusters while it can achieve a manoeuvre in less time than electric thrusters, which shows its potential as a propulsion system.

The following components can be identified in an STP system [11, 23]:

1. Nozzle. This component produces the thrust by expelling heated propellant.

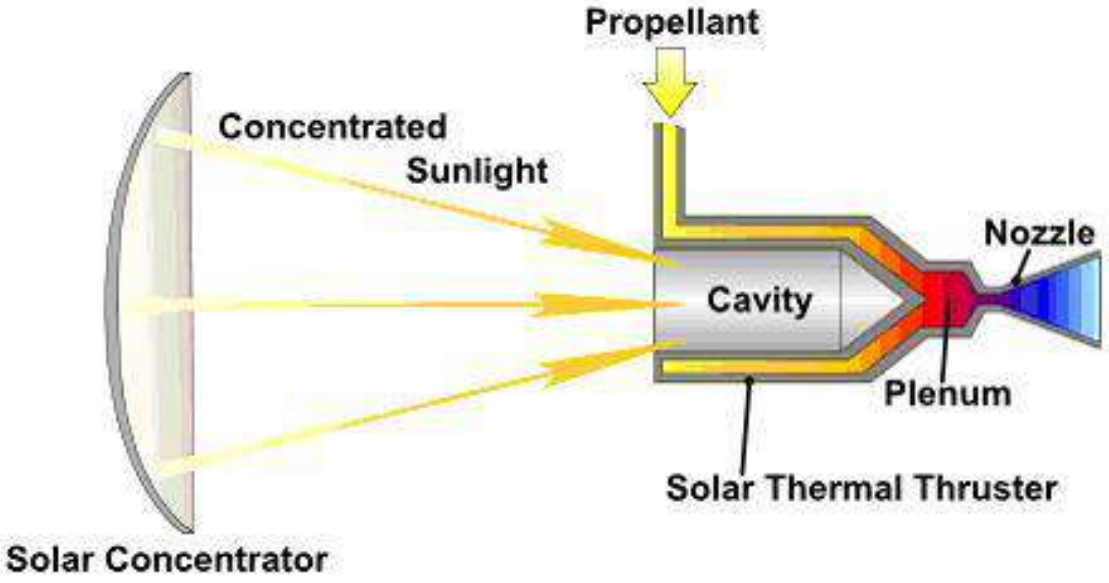

Figure 2.1: Schematic figure of an STP system [4].

2. Concentrator. The Sun heat can be concentrated with the use of one or multiple mirrors and/or lenses. This can potentially increase the efficiency of the system, but also makes it more complex.
3. RAC. This component "receives" the Sun rays and "absorbs" them. Propellant runs through the walls of the RAC. Here, the heat is transferred from the RAC wall to the propellant. Insulation is also included in this component.
4. Propellant tubing (including valves). This determines the layout of the tubing around the RAC.
5. Fiber optical cables. These cables can transport the Sun light to the RAC, which enables the designer to decouple the nozzle and concentrator attitude.
6. Thermal energy storage. A high density, high temperature material (such as graphite [24]) which stores the thermal energy for later usage.
7. Propellant.
8. Propellant tank. To store the propellant.
9. Propellant feeding system. One could think of a blow-down system or a pump fed one. Naturally, both have their own advantages and disadvantages.

2.2. History and research nowadays

Already since the 1950s, research has been conducted in the field of solar thermal propulsion [20]. Traditionally, STP was researched for its high I_{sp} (in the range of 1000 s) [17]. Because of this, tight requirements were introduced on the solar collectors (very large), cost (high) and temperature (in the range of 3000 K, introducing requirements for the used material).

Leverone et al. [11], in their latest article, also presented an extensive overview of the history of STP, starting at the invention in 1956. The overview is described below in some detail. What becomes clear from the overview is the involvement of governmental institutes (e.g. Air Force Rocket Propulsion Laboratory (AFRPL), National Aeronautics and Space Administration (NASA)) in the earlier research towards STP, while later on universities (e.g. Italian, Chinese, Dutch universities) put in efforts to the realisation of STP in spacecraft applications.

STP kicked off with the publishing of the article "The solar-powered space ship" by German scientist Krafft A. Ehricke in 1956 [5]. He argued that the use of chemical propulsion would certainly be necessary for space flight (the space race had yet to start), but that it was limited in the energy supply in the sense that rockets had to carry their own supply of "energy" with them. Thus he proposed, next to a nuclear option, the use of reflector collectors. Already Ehricke sees disadvantages in the structure (heavy) and the rigidity of the design (the collector attitudes and thrust direction are coupled). Furthermore, he saw the merits of hydrogen as propellant and conducted some research towards the specific impulse. In Figure 2.2, the specific impulse is shown as the result of chamber pressure and propellant temperature. The potential of the combination of STP and hydrogen can be deducted from this. The graph was also quickly evaluated using Ideal Rocket Theory (IRT) [25], with hydrogen characteristic inputs, ambient pressure of 0.1 atm (as Ehricke stated) and varying chamber temperatures and pressures. In Figure 2.3, it is shown that this nicely lines up with Ehrickes findings.

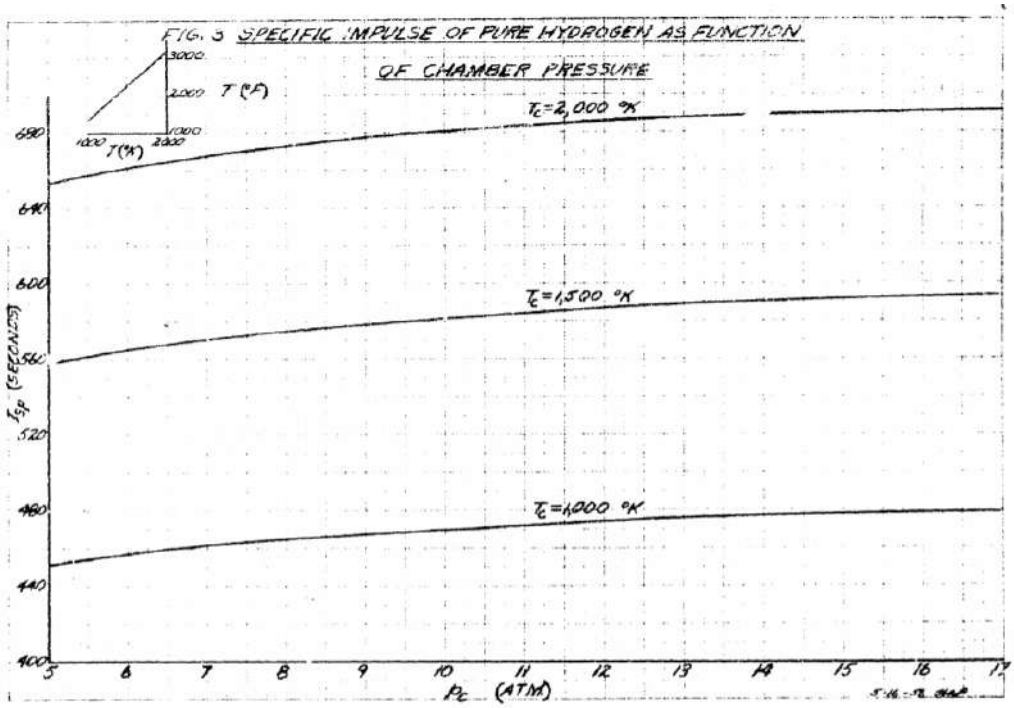

Figure 2.2: Hydrogen specific impulse, dependent on chamber pressure and propellant temperature in STP [5].

In 1962, the paper published by the AFRPL [14] handed the reader one of the greater reasons STP had not been researched further yet: the investments in the concentrator system were deemed too great (and thus too risky), turning the attention towards other means of space propulsion. Even today, the usage of large concentrators (mirrors and lenses) is a huge disadvantage, partly explaining the fact it never flew in space. Next to that, off-axis parabolic mirrors are proposed in this study. Again, the benefits of STP are described, this time by a mission wherein the orbit was raised from Low Earth Orbit (LEO) to Geostationary Earth Orbit (GEO). In Figure 2.4, a comparison is made between chemical, electric and solar thermal propulsion for this (not further specified) mission. In the last column, the large payload increase is shown.

After a jump in time, JM Shoji discussed several propellants in his paper in 1983 [26]. These are: hydrazine, ammonia, methane and hydrogen. Hydrogen turned out to be the best performing propellant due to the high I_{sp}, even at lower temperatures. Furthermore, advice was given regarding the RAC material. Rhenium proved to be a promising material, capable of resisting high temperatures, having sufficient strength and being manufacturable. Carbon was also mentioned, but its manufacturability lacks with respect to rhenium.

Zubrin et al. [27] proposed the bimodal thermionic system (power and propulsion combined) in

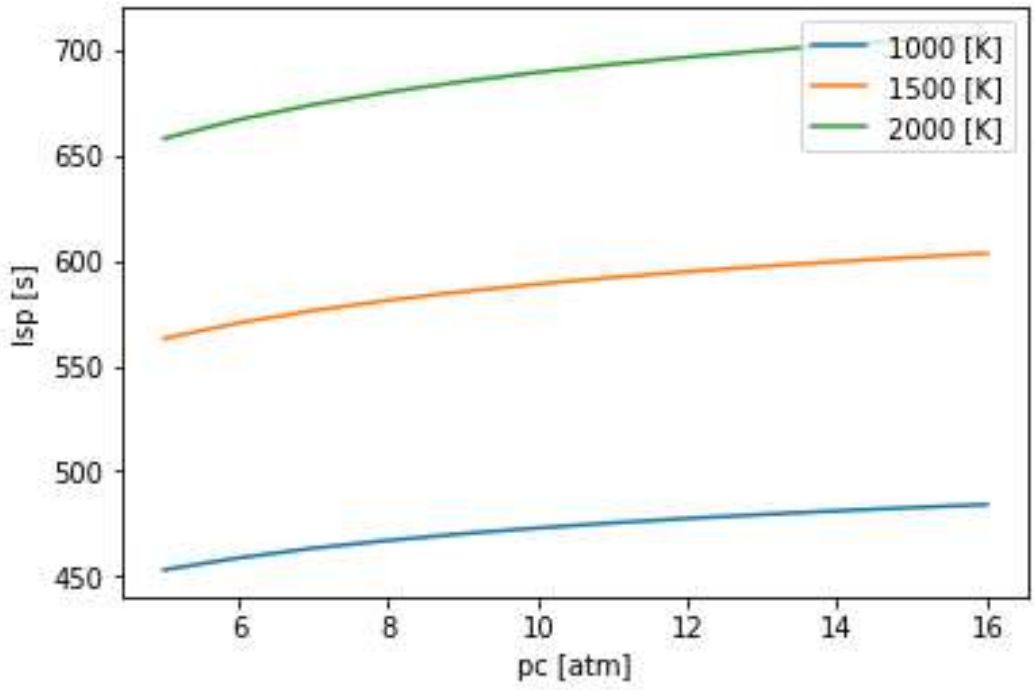

Figure 2.3: Verification of Ehrickes graph using IRT.

	LO_2-LH_2	ION	SOLAR 1	SOLAR 2
V, ft/sec	14,000	19,200	19,200	15,750
Trip Time	5 hrs	180 days	14 days	40 days
Isp, Sec	475	2,940	872	872
Mass Fraction	0.90	0.68	0.85	0.85
Payload, lbs	20,400	44,000	20,500	29,000

Figure 2.4: Comparison between propulsion types for raising the orbit from LEO to GEO.

1992. The system was capable of delivering either 40 kW of power or a thrust of about 111 N at a I_{sp} of 736 s. It can be seen as the predecessor of the bi-modal STP system.

It did not take long for this bi-modal STP system to emerge. In 1994, John Malloy et al. filed a patent for a hybrid solar rocket equipped with a thermal storage [28]. In 1997-1998, another bi-modal system, the Integrated Solar Upper Stage (ISUS) program sponsored by Phillips Lab, had its ground demonstration [12] [13]. Again, in the ISUS program, propellant selection was applied, choosing between hydrogen, methane and ammonia. Furthermore, multiple Earth raising maneuvers are discussed in the papers, e.g. from LEO to a Highly Elliptical Earth Orbit (HEEO). However, the ISUS program and its successor, the Solar Orbit Transfer Vehicle (SOTV) were terminated because of funding issues [29]. Further research into bi-modal systems was mainly done by Gilpin et al. [15, 30, 31], Leverone et al. [11, 32] and Clark [8].

Around the 2000s, Fred Kennedy and Philip Palmer [29, 33, 34] investigated the use of STP for microsatellites at the Surrey Space Centre. They not only did this for Earth orbit maneuvers, but also for interplanetary travel. Kennedy also argued that, while the use of hydrogen as STP propellant would yield the best performance (in terms of specific impulse), large storage volumes and cryogenic storage might cause the system to be too complex. He suggested looking into water or ammonia as propellants

because of these issues.

Furthermore, they discussed the reasons previous STP programs (such as ISUS and SOTV) were not successful. They believed the relatively high complexity of the system, to which the concentrator system was a large contributor, was an issue. Next to that, there was the aforementioned volumetric and cryogenic issues of hydrogen.

In 2003, Japanese scientists Hironori Sahara and Morio Shimizu conducted experimental work with a molybdenum solar thruster, heating the thruster to 2300 K with an I_{sp} of 800 s [35]. They also came up with an interesting advantage to STP: it is more eco-friendly than its chemical counterpart when using e.g. hydrogen or water. Other research in the field of STP for microsatellite applications can be found in [36–39].

Interesting to note is the introduction of fiber optic cables for smallsat applications by Henshall et al. [17, 18] and Nakamura et al. [20] in 2005-2006. The cables solved the issue of the attitude constraint, where the concentrator was fixed with respect to the nozzle.

The last research items that are noteworthy are the discovery of ammonia disassociation at temperatures above 2300 K (which is beneficial for the specific impulse) [40] in 2014 and the application of STP on upper stages of interplanetary spacecraft in 2016 [41]. At DUT, throughout the years multiple theoretical and practical studies are performed, which will be elaborated on in the next section.

2.3. TU Delft research

STP has been researched and is researched at the faculty of AE at DUT. Various examples can be found in Leenders' work, up to 2008 [42]. Thereafter, multiple theses and PhD research were performed. The most important, both theoretical and practical, are:

- In 2006, Harrie Leenders & Peter Batenburg undertook a project towards thermal control of an STP system [43]. In the end, the heating of the propellant in the heat exchanger was most researched. The most notable result of the research was that proper isolation is very much needed due to the high temperatures attained in the exchanger. Furthermore, the absorption coefficient can be altered by using certain paints or coatings. Next to that, an optimum total system mass can be achieved by trading off the length of the motor versus the flow temperature. The longer the propellant runs through the walls of the exchanger, the higher the temperature and specific impulses. This results in a lower propellant mass, but increases the exchanger mass. Finally, a low wall thickness with high thermal conductivity is preferable, but care should be taken that the walls can withstand internal (thermal) loads. Carbon is a good candidate.

  They also constructed a tool which, in short, calculates the propellant characteristics after heating in a heat exchanger. The tool itself is available in Matlab. It is documented extensively, but the tool should be used with care, as not verification or validation is done. It is thus not known whether the values are realistic nor meet the requirements.

- In 2007, Alban Janssens did his thesis towards the design of an STP thruster for a 3 kg nanosatellite [21]. Unfortunately only his paper is available online, the thesis report itself is not. The STP thruster used water as propellant and attained a flow temperature of 1000 K, resulting in an I_{sp} of 201 s. The mass was 149.9 grams and the volume 89.4 cm^3. Janssens added a thermal storage to the system, the resulting deltaV (ΔV) equaled 5 m/s.

  Janssens did not fully state all parameters in the paper. However, using IRT one is able to assess the listed specific impulse. Assuming the ambient to be vacuum, the specific impulse at 1000 K at a chamber pressure of 0.99 bar can be 218.2 s at most. This value corresponds well.

  It is not known whether Janssens made a (preliminary) design of the heat exchanger, which is a missed chance as it is an important part of an STP subsystem.

- In 2007, Leenders conducted a literature study towards the feasibility of an STP demonstration at DUT [23]. In the study, an extensive overview of the technology options of the different engine components was given. This includes research towards lenses, mirrors, optical fiber cables, direct and indirect propulsion, propellant channels, thermal storage, propellant, propellant feeding system and other. Furthermore, an elaborate description of design steps for the thruster is given (complementary with a thermal model in Matlab), followed by a test plan which includes the test facility (at DUT) and components necessary. This literature study could be a welcome source of information for this literature study.
- In 2008, Leenders completed his thesis, which is complementary to the aforementioned literature study [6]. The thesis is divided into 5 main parts:
  - Background of STP, including research done at the faculty of AE at DUT.
  - Design of the thruster.
  - Test plans and testing.
  - Test results, analysis and discussion.
  - Conclusion and recommendations.

  Leenders' thesis is further analysed in Section 2.4. The thesis is important, is it resembles the current thesis and literature study project very well in terms of goals and design steps. From these documents, various recommendations and pitfalls can be taken which could tremendously improve the current project.
- In 2015, JJ Preijde designed a STP system for a small satellite (smallsat) [10, 44]. He altered the usual function that a STP subsystem has. Not only should it provide the propulsion of the smallsat, it should also generate electrical power. The smallsat has a dry mass of 200 kg and a bus volume of 1 m^3.

  His focus point was on the development of a Design, Analysis and Optimization (DAO) tool. This tool first calculated the solar influx based on the current orbit. Using this influx, the temperature at various locations of the thruster were calculated. The eventual design consisted of two concentrators (the first one being an on-axis lens, the second being a refractive lens), cylindrical RAC with spiral tubing. Interestingly enough, nitrogen as a propellant only lowers the thrust by 4% and the the I_{sp} by 2 seconds with respect to liquid ammonia. However, it should be kept in mind that this applies to larger satellites, not the nanosatellites which are under discussion in this report.

  The tool is available in Matlab. The downside is that it is assumed that the wall has a constant temperature, while this will of course depend on the incoming power flux. However, Preijde spent some work on view factors, which is useful in the RAC tool construction (see Chapter 3).
- In 2016, Daniel Martínez Pino designed, manufactured and tested an inflatable concentrator for a PocketQube (nanosatellite, consisting of cubes of $5 \times 5 \times 5$ cm^3) [45, 46]. Next to that, he designed an STP thruster, having over 100 mN of thrust and around 200 seconds of I_{sp}. The propellant is liquid ammonia for having a reasonable performance while having better storability than hydrogen. Testing was described quite extensively, which is used as an example for the test plan in Appendix B.
- In 2017, researchers from the faculty of Aerospace Engineering Leverone, Cervone, Pini et al. [32] published a paper on the bi-modal STP concept which describes a system that provides both electric power and propulsion to the spacecraft. They elaborated on the system design and the Organic Rankine Cycle (ORC), but also added a section on propellant selection. Viable propellants identified are ammonia and water (properties at 600 K). Ammonia has a high specific impulse, due to disassociation into nitrogen and hydrogen at high temperatures (2500 K). It also requires relatively low solar power due to low heat capacity. Water requires less storage volume when similar DeltaV (ΔV) is needed, making it more volumetrically attractive than ammonia. It has an equivalent specific impulse but requires a great deal of solar power due to the relatively high heat capacity. Nitrogen was not discussed.

- In 2018, Krishti Das formulated her thesis objective as to design an STP thruster for CubeSat applications out of MEMS based components [19]. An interesting design consideration was that she advocated a rectangular RAC (in contrast to the more-chosen cylindrical RAC) because of manufacturability. As expected, she makes use of fiber optic cables to decouple the RAC and thruster attitude. Care should be taken when using this thesis as a source, as the design is based heavily on Microelectromechanical Systems (MEMS) components.
- In 2019, Leverone et al. [11] published a paper, containing a comparison between propulsion technologies for smallsats. Next to that, an overview of the current status of STP is given. Leverone describes the current challenges of STP, such as the lack of flight heritage, the need for efficient and lightweight concentrators, research into fiber optic cables and other. In the paper, a design thrust of 1 N and chamber pressure of 2 bar is selected.

2.4. Layout Leenders

In Section 2.3, it was stated that Harrie Leenders has conducted a similar research as the current project. It was thus decided to delve into his thesis more and extract any useful information. Please note that the engine he developed will be called Solar Thermal Thruster 1 (STT1), while the thruster that is to be developed in this project will be named STT2.

Leenders started off with the background of STP, describing the principle of STP, what was already done at DUT and what the relationship of his research was to these previous studies.

It was followed by an elaborate design chapter, where the problem statement was made and the requirements were shown. Here, also the goal of the thesis was stated: "Development a solar thermal propulsion system laboratory technology demonstrator". In other words, Leenders wanted to design, manufacture and test a STP demonstrator. It was specifically stated that no mission was selected, so there were no mission requirements, only qualitative requirements. This was because the goal was to "prove" the feasibility of STP. He continued with various design options regarding the RAC configuration, light source and light concentrating system. Then, a whole section was spent on designing the most crucial component, the RAC. Attention was also given to the propellant choice, which turned out to be gaseous nitrogen. The RAC was designed as a cone.

In the chapter thereafter, he showed the test plans, both for testing the irradiance output of the heat source (a 1000 W theater lamp) as for the thruster itself. The test plans cover the protocols and the test designs. Then he described the test data and the discussion about this data. Again, the data is split into two parts: the irradiance test data and the thruster test data. Thereafter, the test data obtained was compared to the theoretical values. These values were generated to make the design in the earlier stages of the thesis.

In the end, conclusions are drawn with regards to the set goal seen before. The conclusion was that the demonstration was successful and the goal was reached. Several important test outcomes were that the insulated RAC reached a temperature of 750 K and that the maximum propellant temperature was 525 K. Furthermore, some recommendations were given in the chapter. Increasing the power output of the heat source, for instance by changing it for another, could improve the power input of the thruster. Furthermore, making the design leak-tight was a recommendation, as was the idea to change the layout of the (now straight) propellant channels in the RAC. The last advice was to change the design of the whole system, e.g. adding a heat storage medium.

2.5. Critical assessment

It becomes clear that the concept has been explored extensively and its feasibility proved numerous times. The TRL of STP is currently around level 3 [11]. According to Mankins [16], TRL 3 can be

summarized as a characteristic proof of concept being present. Technologies at TRL 3 do benefit from laboratory-based studies towards validation of theoretical models of the performance, which raises the level to 4. Executing a test where components, such as the RAC, are tested are thus needed to raise the TRL level in order to reach 9, where missions are successfully carried out with the use of said concept.

Looking at the TRL level, it is not surprising that STP has never been flown in space yet. Observing the literature described in the latter two section, there are two main disadvantages which could explain the lack of space-borne STP:

1. The need for solar illumination during thrusting. This could be problematic in case of a solar eclipse. However, this disadvantage is mostly mitigated with the use of fiber optic cables and thermal storage. The latter allows for even higher thrust compared to a STP system without thermal storage, because there is the possibility for propellant heating by both direct sunlight and thermal storage.
2. The need for large solar concentrators. While electric propulsion systems rely on batteries and solar panels, STP systems need their own dedicated solar concentrator systems. However, powering the spacecraft by a bi-modal STP system eliminates the need for a dedicated electric generation component.

It goes without saying that, although solutions were found to the problems described above, it dramatically increases the complexity of the whole system. While chemical (and to an extent also electrical) propulsion has been researched, tested and flown numerous times in the last 50+ years, STP has a large investment ”threshold” which it first has to pass to become competitive for (micro)satellite applications.

Furthermore, various propellants are proposed in the earlier sections. Ammonia, hydrogen, water and nitrogen are the most promising of those, for various reasons. In the model coming later, these four will thus be reviewed in terms of specific impulse, thrust and other aspects. For this project, it is expected that gaseous nitrogen will be used, due to its inert nature, intermediate performance and high availability.

What should not be forgotten is that the performance model will become a significant part of this project. It is under construction, but should still be complemented by a thermal model which is now lacking. This part can be based on the Matlab script Leenders constructed a decade ago.

STP having never been flown in space only encourages the idea of designing and building a demonstration tool in order to show the feasibility in real life. When successful, this design could be used as a (demonstrator) propulsion means on a (small) spacecraft, for instance as part of the Delfi program, run by DUT [47].

3

Solar Thermal Propulsion tool

This chapter will describe the tool used to predict the performance of the solar thermal thruster. It will be called the Solar Thermal Propulsion tool, or STP tool. There are three distinct sections in this chapter, each describing the literature related to one particular part of the thruster. The first one revolves around the feed system, containing the propellant that will be used to create thrust. It will assess the mass and size of the feed system. The second part will be about the most influential segment of the thruster, namely the RAC or heat exchanger. It will determine the outgoing propellant temperature and heat exchanger efficiency. Afterwards, the third tool (the nozzle & performance tool) will describe the nozzle dimensions and ensuing performance, in terms of thrust and specific impulse, based on the propellant temperature outputted by the previous tool.

Each of these three sections will show available literature which will clarify certain choices that were made in the tool design. Furthermore, an example of inputs and outputs is given, which will be commented on. Next to that, suggestions are given at the end of each section how to improve the particular tool to make it more realistic. The final section will contain a summary of the most important findings of the chapter.

The tool will be used to assess the impact of design choices when an STP thruster is designed. It will e.g. show the effect of applying insulation, or it will show what happens when more input power is delivered. In that way it will be valuable to the user.

3.1. Feed system tool

In this section, the feed system tool for the STP thruster will be described. The feed system is divided into two sections; first, the tank will be assessed, followed by a section on the tubing from tank to RAC. In the end, there will be a section holding recommendations for further tool expansion.

Four propellants were selected for evaluation, based on the literature review: gaseous nitrogen, gaseous ammonia, liquid water and gaseous hydrogen.

3.1.1. Feed system tank

For a feed system, two main options exist: the pressurized-tank system and the pump-fed system. From Zandbergen [25], it becomes clear that the latter is mainly used in high-impulse, high-thrust missions, while the pressurized-tank system is normally seen under the opposite. Because the tank

is designed for STP microsatellite applications, a pressurized-tank system will be chosen. The same reasoning was applied by e.g. Preijde [10] for his thesis in 2015. Note that other feeding systems, such as capillary or gravity feeding, are not treated to keep the tool simple.

There are two principal pressurized-tank systems: the blow-down type and the regulated system one. The first incorporates a pressurant in the tank, divided by e.g. a diaphragm. The latter has a separate pressurant tank, regulated by a regulator valve. The first one has the advantage of limited amount of components, but suffers from high tank mass due to the pressurant being in the same tank as the propellant. The latter experiences the opposite, making it less reliable. However, the regulated system has the advantage of lower tank mass. Again, to simplify the tool, the blow down system is opted in order to reduce the amount of components. Furthermore, the pressurant will not be heated nor will the propellant be cooled to cryogenic temperatures, to reduce the amount of components.

Various relations exist to calculate the tank mass, of which a few are listed in [25]. Unfortunately, the given methods mostly exist for large (1000's of kg) propellant tanks, which are not usable for micropropulsion applications. However, a preliminary sizing of the propellant tank is still possible, using a few assumptions:

1. The tank will be designed for gaseous propellants. This has the consequence that the propellant can be pressurized.
2. The tank will be cylindrical with spherical end caps. Cylinders are beneficial in terms of wall thickness (low) and spacecraft volume implementation.
3. The propellant will expand isothermally, as the used propellant will have low pressure (below 1.0 MPa) so the expansion can be assumed slow.

The feed system mass (M) is then composed of the following masses:

$$M_{feedsystem} = M_t + M_p + M_g + M_{tubes} + M_{remaining} \tag{3.1}$$

Where the subscripts are tank (t), propellant (p) and pressurant gas (g). The propellant mass is usually known when designing a feed system, as it is derived from the mission characteristics on velocity increment. The tank mass and pressurant mass are discussed in this subsection, the tubes and remaining mass in the subsection hereafter.

To calculate the tank mass, first the pressure inside the tank should be found. The minimum feed pressure p_{feed} in the propellant tank can be related to the desired chamber pressure p_c (where the subscript is chamber (c)) assuming a pressure loss margin in the feed lines from tank to RAC $p_{l,tank->RAC}$, RAC tubing $p_{l,RAC}$ and feed line losses from RAC to chamber $p_{l,RAC->chamber}$:

$$p_{feed} = p_c + p_{l,tank->RAC} + p_{l,RAC} + p_{l,RAC->chamber} \tag{3.2}$$

Here, the subscript is loss (l). The desired chamber pressure is set at a somewhat arbitrary 2.0 bars, which is proposed by Leenders [6] and Preijde [10]. In Section 3.2 (on the RAC), the latter two losses will be discussed. In the next subsection, the remaining pressure loss (from tank to RAC) is described.

When the desired feed pressure is known (using Equation 3.2), one can start designing the tank. In the tank, both pressurant and propellant are present, divided by an active element, e.g. a diaphragm. From [25], the ratio between the propellant and gas is given in Equation 3.3 as the blow down ratio (B).

$$B = \frac{V_g + V_p}{V_g} \tag{3.3}$$

A blow down ratio between 1.5-2.5 is usually encountered [25], but ratios of 4.0 [48, 49] or even 5.0 [10] are not unheard of. Leenders unfortunately did not report any on this.

At the end of propellant tank emptying, the pressurant gas should have the minimum pressure $p_{g,f}$ equal to the propellant pressure (Equation 3.4). So initially, the pressurant gas pressure $p_{g,i}$ should be higher, according to Equation 3.5. Here, the subscripts are initial (i) and final (f).

$$p_{g,f} = p_{feed} \tag{3.4}$$

$$p_{g,i} = B \cdot p_{g,f} = B \cdot p_{feed} \tag{3.5}$$

Knowing the initial gas pressure, the cylindrical tank wall will be designed for that pressure. The propellant volume, pressurant volume and total tank volume can be calculated using Equations 3.6-3.8, where universal gas constant (R_A), molar mass (MM) and temperature (T) for the tank.

$$V_p = \frac{M_p \frac{R_A}{MM_p} T}{p_{feed}} \tag{3.6}$$

$$V_g = \frac{V_p}{B - 1} \tag{3.7}$$

$$V_t = V_p + V_g \tag{3.8}$$

Having the tank volume, the pressurant gas mass can be assessed via the following equation:

$$M_g = \frac{p_{g,f} V_t}{\frac{R_A}{MM_g} T} \tag{3.9}$$

The tank mass can be calculated using five relations, see Equations 3.10-3.14. In the first equation, the cylinder wall thickness is calculated using the aforementioned pressurant pressure, shell radius (R), yield stress (σ) and safety factor (j) [25]. The tank is assumed thin-walled (thickness (t) « R). The thickness for the spherical end caps is a factor 2 smaller. The second equation gives the tank volume, based on geometrical equations. Then, in the third equation (Equation 3.12), the tank shell mass is calculated using the density (ρ). Finally, Equation 3.13 will give the total tank mass $Mass_t$, using the shell-to-tank factor (K). The factor ranges from 1.2-2.5 [25], with the tendency to be higher for lower volume tanks (< 100 liters). The factor implements the effect of propellant management devices, in/outlet provisions and mounting provisions. A relation is actually given, but it should be used with extreme care, as it is applicable for spherical titanium tanks with a diaphragm. Nonetheless, as no other relation can be found, it is used in Equation 3.14.

$$t = \frac{p_{g,i} R}{\sigma} \cdot j \tag{3.10}$$

$$V_{shell} = \pi \left(R^2 - (R-t)^2\right) \cdot L + \frac{4}{3}\pi \left(R^3 - \left(R - \frac{t}{2}\right)^3\right) \tag{3.11}$$

$$M_{shell} = V_{shell} \cdot \rho \tag{3.12}$$

$$M_t = K \cdot M_{shell} \tag{3.13}$$

$$K = 6.84 \cdot (V_t \cdot 1000)^{-0.2067} \tag{3.14}$$

The only geometrical restrictions on the tank are that it has to hold the volumes of both pressurant and propellant while being cylindrical. The cylindrical length (L) (without end caps) and R are thus not restricted. What is observed, is that the lowest tank mass is attained when the tank length is zero (e.g. a spherical tank), which is not surprising. To set a restriction, a ratio between length and radius is set, for now at 2.0, meaning that the cylinder length is twice the radius of the tank.

3.1.2. Feed system tubing

It is extremely difficult to design the feed system tubing when no mission is selected. Still, to get an idea of the ballpark figure, Zandbergen [25] states that the plumbing mass is between 7.0%-17.6% of the total propulsion system dry mass for 65% of the times. Keep in mind that these numbers apply for the total system, not only the tank. For now, a percentage of 20% of the dry tank mass is assumed, so:

$$M_{tubing} = 0.20 \cdot M_t \tag{3.15}$$

Determining the pressure loss in the tank-to-RAC tubing $p_{l,tank->RAC}$ proves equally challenging, with minor data available. Again, Zandbergen provides some means to get a figure, but without a detailed tubing outline, an estimation has to be made. What can be concluded, is that a higher mass flow also increases pressure drop, while a higher feed pressure gives a lower pressure drop. The exact numbers are not useful, as the mass flow at which they are assessed lies at 10 g/s, while the STP demonstration mass flow will be below 1 g/s (Leenders employed 300 mg/s [6]). Preijde [10] found a pressure drop of 1.28 bar for a chamber pressure of 1.00 bar, setting the feed system propellant pressure at 2.28 bar. It it thus decided to equate the pressure drop for the tubing from tank to RAC plus the pressure drop from RAC to chamber at 100% of the desired chamber pressure, see Equation 3.16.

$$p_{l,tank->RAC} + p_{l,RAC->chamber} = 1.00 \cdot p_c \tag{3.16}$$

This also simplifies Equation 3.2 to:

$$p_{feed} = 2.00 \cdot p_c + p_{l,RAC} \tag{3.17}$$

3.1.3. Feed system tool example calculation

In Tables 3.1 and 3.2, the inputs and outputs for this part of the tool respectively are given. What becomes clear from the outputs, is that the tank mass is relatively high compared to the propellant mass. This design would not be feasible for e.g. CubeSats (a type of microsatellite) as they are limited in volume and mass. The volume can be adjusted by increasing the initial pressure, which would of course result in thicker tank walls, keeping the mass at approximately the same level. A regulated system has better (lower) mass characteristics, but will be more complex.

What would be an improvement is the use of liquid propellant, instead of gaseous. Liquids have higher densities, lowering the volume (and thus the wall thickness). Disadvantage is that the propellant might have to be cooled, introducing boil-off and isolation issues. Preijde (see below) [10] shows the effect of having a liquid propellant.

Inputs			
Name	**Symbol**	**Value**	**Unit**
Propellant	-	Nitrogen	-
Propellant mass	M_p	0.500	kg
Chamber pressure	p_c	$2.0 \cdot 10^5$	Pa
Tubing pressure loss	$p_{l,tank->RAC} + p_{l,RAC->chamber}$	$1.00 \cdot p_c$	Pa
RAC pressure loss (assumed for now)	p_l, RAC	$0.3 \cdot 10^5$	Pa
Temperature	T	298.15	K
Blow down ratio	B	4.0	-
Tank material density	ρ	2810	kg/m^3
Pressurant gas molar mass (helium)	MM_g	$4.003 \cdot 10^{-3}$	kg/mol
Length-to-radius factor	c	2.0	-
Safety factor	j	2.0	-
Universal gas constant	R_A	8.314	kg/K/mol
Propellant molar mass (nitrogen)	MM_p	$28.0134 \cdot 10^{-3}$	kg/mol
Enthalpy values propellant (nitrogen)	-	-	J/kg

Table 3.1: Feed system tool: example inputs.

Outputs			
Name	**Symbol**	**Value**	**Unit**
Propellant volume	V_p	0.103	m^3
Pressurant volume	V_g	0.034	m^3
Tank volume	V_t	0.137	m^3
Pressurant mass	M_g	0.095	kg
Tank radius	R	0.24	m
Cylinder length	L	0.47	m
Tank material volume	V_{shell}	0.00176	m^3
Shell mass	M_{shell}	4.96	kg
Tank-to-shell ratio	K	2.47	-
Tank mass	M_t	12.26	kg
Initial gas pressure	$p_{g,i}$	$17.2 \cdot 10^5$	Pa
Tubing mass	M_{tubing}	2.45	kg

Table 3.2: Feed system tool: example outputs.

Looking at the previous thesis students involved in STP at DUT, Preijde reported a dry tank mass of 2.1 kg for 29.3 kg of propellant (liquid ammonia at 240 K) [10]. Note that the tool should be slightly adjusted because the propellant is in liquid state, not in gaseous state. Checking [50], liquid ammonia has a density of approximately 683 kg/m^3. The other stated values in his thesis are a blow down ratio

of 5.0, a tank volume of 0.052 m^3, a temperature of 240 K, tank radius of 0.176 m, tank cylindrical length of 0.30 m, material density of 2700 kg/m^3, material yield stress of 276 MPa and a constant thickness of 1.1 mm (also at the spherical end caps). This yields the results, stated in table 3.3. As can be seen, the values are mostly similar. The greatest difference is in the tank mass, due to a slightly different use of equations. What should also be observed is the great decrease in tank mass in comparison to a gaseous propellant. Cooling the propellant can, at the cost of more complexity, greatly affect the mass budget.

Leenders [6] did not design a feed system, hence no verification can be done using his thesis. Das [19] lists a tank mass of 1.5 kg for 1.85 kg of propellant, but elaborates no further than "rough calculations". Pino [45] has not evaluated the feed system as well.

Name	Symbol	Unit	Value (Preijde)	Value (feed system tool)
Thickness	t	m	0.0011	0.0013
Pressurant mass	M_g	kg	0.0232	0.0245
Pressurant volume	V_g	m^3	0.0104	0.0107
Tank shell mass	M_t	kg	2.10	2.53
Propellant volume	V_p	m^3	0.0416	0.0429
Surface area	S_t	m^2	0.72	0.72

Table 3.3: Comparison Preijde and feed system tool [10].

3.1.4. Feed system tool recommendations

A few recommendations to further expand the tool are listed here.

1. Incorporate other feed systems, such as pressurized systems and pump-fed ones. The first is more important than the second, because pump-fed systems are rarely seen in low-impulse missions [25].
2. Implement the effects of pressurant heating or propellant cooling.
3. Implement liquid propellant options.
4. Further explore the tank-to-shell ratios.

3.2. RAC tool

The RAC is an essential part of an STP thruster; it transfers the solar energy towards the propellant. It goes without saying that an efficient transfer is required to heat the propellant sufficiently and elevate the performance.

There are various design choices which should be decided on for the RAC; the configuration, the material, the shape, the tubing lay-out and the insulation will be shortly described in the following subsections.

It should be noted that the tool developed here is for very specific uses only, primarily because the used heat source does not resemble solar light in terms of spectral and bundle size characteristics. For the more general tool, one is directed to Preijde [10], who did a theoretical study towards STP, which also involved the development of a very detailed model including a part on the RAC.

What also should be kept in mind, is that the actual design choices will be made in the thesis following after the literature study. This section will merely explain the tool which will be used for that

purpose on the basis of literature. A huge impact on the issues described here are the literature studies and theses performed by Leenders [6, 23] and Preijde [10, 44].

3.2.1. RAC configuration

As Leenders [23] and Das [51] pointed out, there are three configurations for the RAC available. These are:

1. Direct propulsion with direct absorption.
2. Direct propulsion with indirect absorption.
3. Indirect propulsion with indirect absorption.

Direct propulsion holds that the heated propellant is immediately used to propel the spacecraft. In other words, the solar irradiation falling on the RAC will not be stored. On the other side there is indirect propulsion, which means that the solar energy will be stored in a medium or a thermal storage. The energy can then be built up and released in a later phase, when thrust is needed.

Direct or indirect absorption depends simply on the manner how solar irradiation is collected. When it falls directly on the propellant, it is called direct absorption. If there is a physical barrier (such as an RAC wall) present between irradiation and propellant, it is indirect.

An example of direct propulsion with direct absorption is a cavity containing a transparent window, with propellant flowing inside the cavity. The propellant is heated and immediately propelled. Another interesting application of this configuration is the rotating bed concept, discussed by Das [51] from Shoji [7]. It relies on a mechanical rotating 'bed', which pushes the propellant against the walls increasing the convective heat transfer. It has a relatively well performance, however the complexity increases drastically due to extra moving parts.

An example of direct propulsion with indirect absorption is the same as the previous example, except for the fact that the irradiation does not fall on the propellant, but there is e.g. an RAC wall inbetween those. The RAC Leenders designed and manufactured in his thesis [6] is a good example of this. The third option, indirect propulsion with indirect propulsion, could be a thermal storage which stores the solar energy and releases it when thrust is needed.

There are various advantages and disadvantages to the three configurations. Indirect propulsion has the huge advantage that it can be decided when thrust can be used. For instance, in orbit raising missions (a not uncommon application for STP spacecraft [11]), the most efficient maneuver (velocity increment-wise) is an impulse at the periapsis of the orbit (so-called Hohmann transfers). For direct propulsion this forms a problem, as this will release the propellant when it is heated, introducing relatively high gravity losses when compared to indirect propulsion. Furthermore, it was proven by Leenders [23] that the thrust-to-collector radius is higher for indirect propulsion than for direct propulsion. Next to that, direct propulsion is useless in case of an eclipse. On the other hand, indirect propulsion has the disadvantage of added mass and complexity because of the thermal storage.

Looking at direct propulsion at the two configurations, direct absorption 'skips' the step of heating an intermediate physical barrier, having no losses there. Indirect absorption of course has to deal with this loss. On the other hand, indirect absorption has slightly less complexity due to the fact it can contain the propellant in flow channels, while direct absorption has to rely on a transparent window.

Leenders [6] employed the direct propulsion with indirect absorption configuration, after a trade-off having 'complexity' and 'performance' as criteria, see Figure 3.1. Preijde [10] also has the same configuration, although it is unclear how he traded-off this concept with regards to the other two. Das [19]

employs the configuration as well, complemented with a fibre optic cable, having listed the advantages and disadvantages. She concluded that the high complexity of the direct absorption was too disadvantageous. James M. Shoji, a researcher at Rocketdyne in the 80s, came to the same conclusion in his overview report [7]: a windowless heat exchanger cavity configuration has intermediate performance, but minimized the risks of complexity and cost.

	Complexity	Performance
Indirect propulsion with indirect absorption	Thermal storage medium yellow	Highest thrust green
Direct propulsion with indirect absorption	Open cavity and no thermal storage medium green	Lower temperature and thrust blue
Direct propulsion with direct absorption	Cavity with window yellow	Highest temperature green

Figure 3.1: RAC configuration lay-out by Leenders [6].

The tool will thus be focused on a windowless cavity configuration, wherein propellant flows through the walls of the cavity while the cavity is simultaneously illuminated by radiation.

3.2.2. RAC shape

Now that the configuration has been determined, there are various RAC shapes to choose from. Shoji [26] listed six concepts, see Figure 3.2.

Shoji introduces a way to evaluate those concepts, which was also described by [51] in her literature study, Section 2.2. It involves a number of variables, such as dimensions, temperatures, view factors and emissivities. However, the method he proposes lacks a thorough explanation. After doing a small sensitivity analysis on the equations, it was found that the outputted values largely made no sense or were too influential. Next to that, the given graphs (by Shoji) were too hard to read, so they could not be checked. This renders the tool largely unreliable, furthermore so because Das rightly pointed out that the evaluated dimensions were not suitable for nanosatellite applications, as they were too large.

It should thus be noted that the conclusions drawn by Shoji should be handled with great care, as the ways to come to these conclusions are not checked. Still, they are needed as not many references exist with such a thorough evaluation of efficiencies of RAC shapes.

Shoji evaluated the six concepts by looking at total performance, total surface area and ease of manufacturing. For the first criterion, he found that the spherical/horn/disc shape did best, followed by the lipped cylinder/disc and the lipped cylinder/horn and the open-ended cylinder. The lipped cone performed best on total surface area (having the lowest, which relaxes the mass budget), followed by both cylinders and the spherical/horn/disc shape. He does not further elaborate on the ease of manufacturing criterion.

Based on the criteria, Shoji concludes that an open-ended cylinder and spherical/horn/disc shape are most promising. It should be noted here that the performance includes that irradiance is not focused on the aperture. So, if the aperture is too small, he sees this as a (partial) loss of solar energy. Nowadays, the concentrators can fix this issue by carefully designing the aperture to incorporate all the focused radiation.

Looking at other DUT students, Das [19] only evaluates a rectangular and trapezoidal shaped RACs,

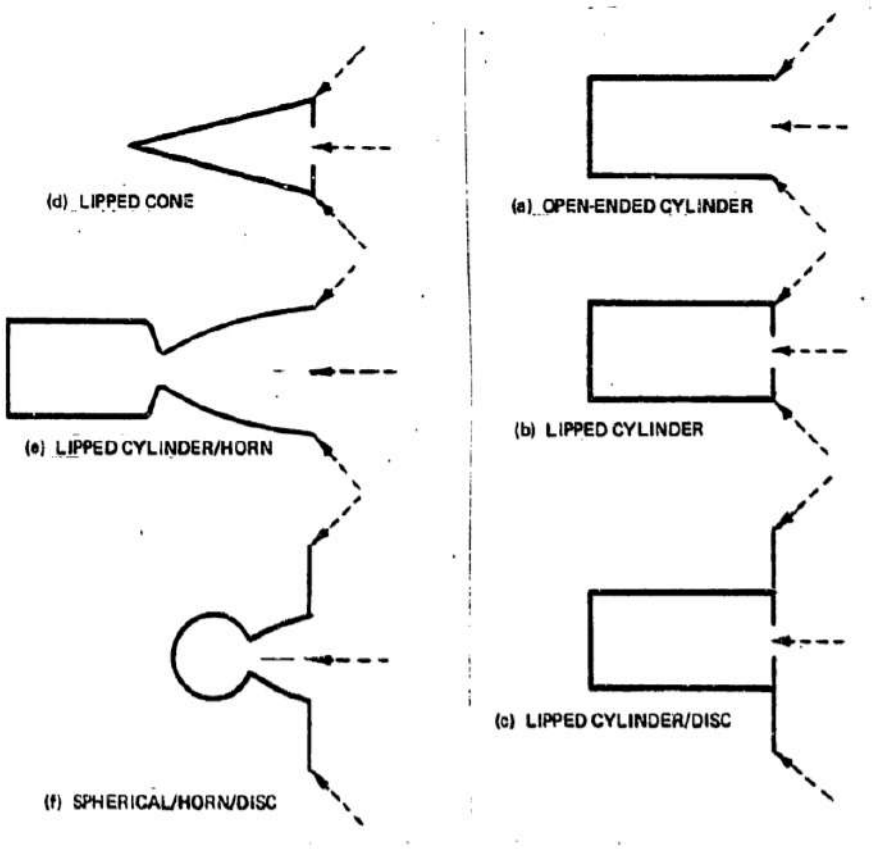

Figure 3.2: RAC shape concepts by Shoji [7].

due to ease of manufacturing. Eventually (as part of a more extensive trade-off) she chooses the rectangular RAC. Leenders [6] does a trade-off for windowless heat exchangers, having a flat plate, cylindrical and conical shaped RACs as options. There, he concludes that the superior temperature distribution of the conical shape beats the cylindrical shape, despite the fact the the cylindrical RAC has lesser reflection losses. Thus, he chooses the conical type. Pino [45] does not elaborate on his choice for a flat plate heat exchanger, only that it is simple and lightweight. Preijde [10] chooses the cylindrical RAC after an extensive trade-off, out of six concepts.

Based on the information above and to keep the tool simple and effective, the tool will evaluate cylinder shapes, as they turn out to be effective, easily manufacturable and often chosen. In Figure 3.3 [8], the temperature distribution over such a heat exchanger is shown following from a ray-tracing program.

3.2.3. RAC tubing lay-out

For the lay-out, roughly two options are outlined in various theses [6, 10]: there is the linear tubing and the spiral tubing. The first has the advantage of less complexity compared to spiral tubing, while the latter has a longer flow path with respect to linear tubing, increasing the propellant temperature. This immediately gives away the choices of respectively Leenders (linear tubing) and Preijde (spiral).

To keep the tool simple, only linear tubing will be implemented.

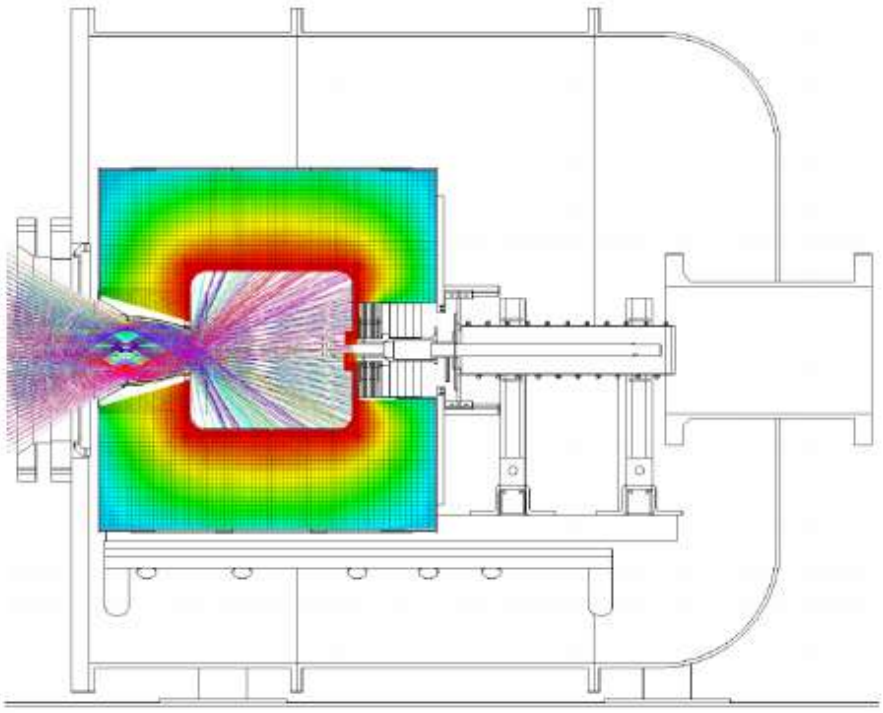

Figure 3.3: Ray-tracing figure from [8], showing the temperature distribution over the RAC.

3.2.4. RAC material

For the RAC material, there are many options listed in literature. Leenders [23], but also Das [51], made an overview of different materials, using criteria such as thermal conductivity, melting point, manufacturability, specific heat of the material, density and thermal expansion.

To ensure a high heat transfer to the propellant flowing through the RAC, a high thermal conductivity is necessary. A high melting point will prevent the heat exchanger from melting under the concentrated solar irradiation, while manufacturability keeps track whether a material can be shaped into an RAC form. The specific heat of the material is important as users want this to be low to prevent the RAC from taking up too much heat which could otherwise be directed towards the propellant. A low density is preferred to keep the heat exchanger mass low, while the thermal expansion needs to be low to prevent the RAC from creating thermal stresses at the interface with other materials (such as insulation) during heating.

Taking these criteria in mind, molybdenum proved to be a promising material, due to its low specific heat, high melting point and high conductivity (also endorsed by [7, 10, 37]). For the same reasons (and by the same researchers), tungsten is seen as a viable material option as well. Rhenium is also considered, but has the downside of relatively low conductivity. All three materials listed here are regarded as high cost, which naturally is a downside.

3.2.5. Insulation and coatings

As will be shown in the next section, insulation of the heat exchanger is vital to ensure that minimal heat is lost via radiation on the outside of the RAC. On the inside, radiation loss is also encountered, but this is mostly mitigated because it is reflected towards another wall of the RAC (hence why cavity shapes are well-liked). Convection is not considered in this tool, as it is assumed to operate in space, where there is no (or minimal) medium present to which the heat will flow through convection.

For insulation, Multi-Layer Insulation (MLI) is recommended [10, 23, 52]. Originally designed to prevent cryogenic propellant tank boil-off, it consists of multiple layers of aluminized mylar, interspaced by low-conductivity material [53]. Because of the multiple layers, the emissivity can be very low on the outside RAC, with a minimum of 0.000 25 [10] reported. Next to that, graphite felt and a combination fiber and phenolic foam [19, 23] are encountered. Requirements for MLI are low conductivity, low emissivity, low density and high melting point.

Coatings on the inside of the heat exchanger are necessary to raise the absorption of the RAC material, thus absorbing more solar irradiation which will raise the propellant temperature (increasing performance). Leenders [6] used black paint for this purpose, however it turned out that the paint was not heat-resistant during testing, although it was listed to be so. Preijde [10] reports the same, as he designed the RAC having carbon black paint, raising the absorptance to 0.96 and the emissitivity to 0.88.

Welding technician Van Slingerland (see Chapter 4) provided a graph to show the absorptivity of different material as a function of wavelength (see Figure 3.4). In the infrared spectrum (in which his welding laser operates), the absorptivity is not terribly high, which again shows the necessity of some sort of coating on the RAC inside.

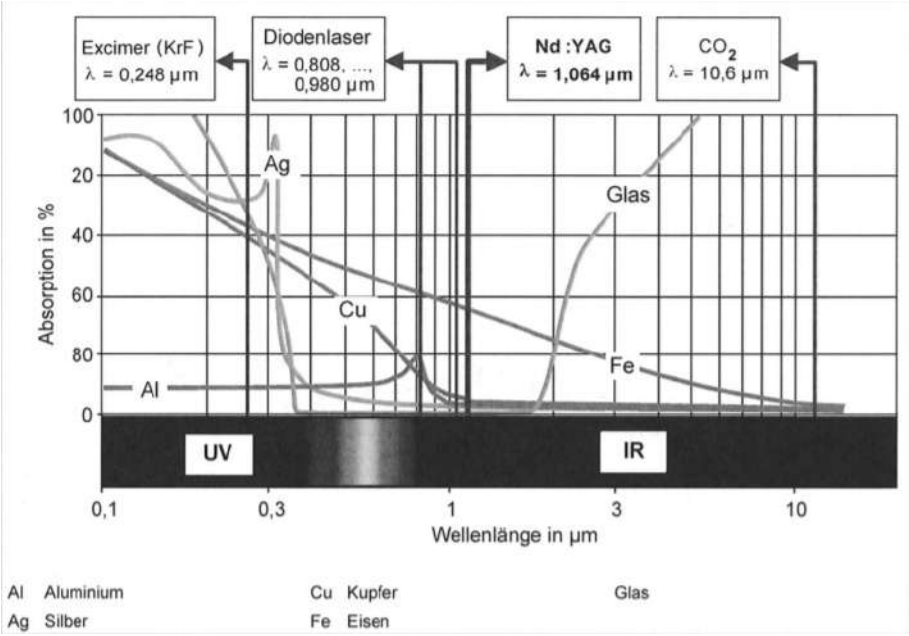

Figure 3.4: Absorptivity of different metals as a function of wavelength.

3.2.6. RAC tool

A tool which can predict the heat exchanger efficiency based on design choices is a valuable asset. In this section, it is explained how the RAC tool is set-up, what inputs and outputs it has, the assumptions and the mathematical expressions behind the tool.

For an extensive RAC thermal analysis, Leenders and Batenburg constructed a useful tool (in Matlab), available at [43], calculating the heat transfer to the propellant. They assumed a cavity-type RAC, filled with an inert gas which is heated to a constant homogeneous temperature. This way, the walls could also be modelled as homogeneously warmed up. They modelled the channels as one-dimensional tubes, where the temperature only varied from the start of the tubing to the end. They split up the tubing in n elements, where all elements are assumed steady state to simplify the equations. Furthermore, at the back-side of the channels (away from the heated RAC inner wall), no thermal losses were assumed.

This tool can very well be incorporated in the tool for this literature study. For that, it needs to be translated to Python syntax. Furthermore, some assumptions need to be changed; first of all, the assumption of a hot inert gas in the RAC will be emitted and replaced by radiation heating. Next to that, thermal losses at the radial outside of the channels will be introduced, although these will be kept low through some form of insulation.

Pino [45] also features a thermal model for the heat exchanger, but he does the (rather large) assumption that he knows the exchanger efficiency. The tool is thus not usable, as the exchanger efficiency will not be an input to the tool here, because it depends on many factors, such as shape, tubing lay-out, paint, emissivities, dimensions and propellant characteristics.

The following assumptions apply for the RAC tool:

1. The RAC is modelled as two flat plates with the propellant tubing running inbetween. One of the sides is illuminated.
2. The RAC is divided into n elements of the same length, just as with the tool of Leenders and Batenburg [43].
3. The tool consists of two steady-state heat transfer problems. The first one is from RAC inner wall through the RAC material to the inner tubing wall. The second is from the outer tubing wall, through RAC material, to the outer RAC wall. Both are assumed to be in steady state for the element that is analysed.
4. The only heat losses are radiative and reflective losses, as no medium around the RAC is assumed (mitigating convective heat loss). On the back side, the radiative heat loss will be minimized by insulation, effectively lowering the emissivity.
5. No heat transfer between elements is assumed.
6. Both RAC, ambient and propellant start at room temperature.
7. The tool will not incorporate heating without propellant flow. So at the moment irradiance falls on the RAC, propellant will flow.

The tool is based on theory described by Zandbergen [25]. It starts off with the input power (P_{in}), after which it is multiplied by the absorptance of the RAC inner wall absorption (α). This power is divided equally over the number of elements (n) and the number of channels (m), which leaves room to later quantify the varying power per element. Because the tubing diameter diameter $(D)_{tub}$ and tubing length L_{tub} are known, the heat flux (q) to one element is known, see Equation 3.18.

$$q_{in,oneelement} = \frac{P_{in} \cdot \alpha}{m \cdot D_{tub} \cdot L_{tub} \cdot n} \tag{3.18}$$

This input flux will then be divided into radiative heat loss at the inside $q_{rad,0}$ and conductive heat transfer $q_{cond,0}$ towards the tubing. The conductive heat transfer will then heat up the propellant via convection $q_{conv,0}$. These transfers are governed by Equations 3.19-3.22.

$$q_{in,oneelement} = q_{rad,0} + q_{cond,0} = q_{rad,0} + q_{conv,0} \tag{3.19}$$

$$q_{rad,0} = \epsilon_0 \sigma \left(T_{innerwall} - T_{amb}\right) \tag{3.20}$$

$$q_{cond,0} = k_{RAC} \frac{T_{innerwall} - T_{tubinginnerwall}}{D_{RAC}} \tag{3.21}$$

$$q_{conv,0} = h_{\alpha} \left(T_{innerwall} - T_{tubinginnerwall} \right) \tag{3.22}$$

Where Stefan-Boltzmann constant (σ), emissivity (ϵ) and coefficient of convective heat transfer (h_{α}). Solving these four equations (also see [43]) will yield the steady-state temperatures for the RAC inner wall and the tubing inner wall, while simultaneously outputting the convective heat transfer towards the propellant $q_{conv,0}$. The same equations apply for the other side of the tubing wall, which in turn outputs the temperatures on that side of the tubing wall and the outgoing propellant convective heat $q_{conv,0}$. For one element, the propellant heat transfer power gain is thus:

$$P_{conv} = \left(q_{conv,0} - q_{conv,0} \right) \cdot \frac{L_{tub} D_{tub}}{n} \tag{3.23}$$

Dividing this power by the mass flow and the number of channels, the enthalpy (energy) gain of the propellant is known. Starting at room temperature, the resulting propellant temperature gain after the first element is then known (through values from National Institute of Standards and Technology (NIST) [50]), after which one can move on to the second element, doing the same calculations. At the same time, the propellant pressure loss (see Equation 3.26) is assessed using the Reynolds number (Equation 3.24) and the Moody friction factor (Equation 3.25), resulting in a (minor) pressure loss in the tubing [25]. There are the propellant velocity (v), dynamic viscosity (μ), Moody friction factor (f), D_{tub} as the element tubing diameter and L_{tub} as the element tubing length.

$$Re_{tub} = \frac{\rho v D_{tub}}{\mu} \tag{3.24}$$

$$f = \frac{64}{Re_{tub}}, Re_{tub} < 2320 \tag{3.25a}$$

$$f = 0.316 \left(\frac{1}{Re_{tub}} \right)^{0.25}, 2320 < Re_{tub} < 10^4 \tag{3.25b}$$

$$f = 0.184 \left(\frac{1}{Re_{tub}} \right)^{0.2}, 10^4 < Re_{tub} < 10^6 \tag{3.25c}$$

$$p_{loss,tubing} = f \frac{L_{tub}}{D_{tub}} \frac{1}{2} \rho v^2 \tag{3.26}$$

Eventually, after the last element cycle has been completed, the final propellant temperature is known and the heat exchanger efficiency can be calculated. The efficiency is defined as the ratio of the enthalpy change of the propellant to the inputted power.

Appendix A shows the Python script.

3.2.7. RAC tool example calculation

In Tables 3.4 and 3.5, respectively the inputs and outputs for the RAC tool are given. Furthermore, in Figure 3.5, the temperatures are given, where $T0$ is the inner side of the RAC inner wall, $T1$ the outer

side of the RAC inner wall, T_p is the propellant temperature, $T2$ is the inner side of the outer RAC wall and $T3$ is the outer side of the outer RAC wall.

As can be seen, the resulting exchanger efficiency is on the low side. Percentages up to 80 percent are reported for (theoretical) heat exchangers [29], whereas here 21.9% is reported. This is mainly due to the large radiation losses at the inner RAC wall due to the high wall temperature $T0$. In reality, this is partly mitigated because the reradiated energy is absorbed by an opposing wall. Implementing this phenomena in the tool is out of the scope of this literature study.

It is also shown that the wall temperatures which belong to the same wall have largely similar temperature profiles, because of the high material conductivity. When the conductivity is lowered drastically, differences between $T0$ and $T1$ and $T2$ and $T3$ on the other hand are observed.

Next to that, the pressure loss is relatively low in the tubing, partly because the tubing is assumed to be smooth. A rough tubing increases the pressure losses but potentially increases the heat exchange.

Finally, the outer wall emissivity is also of importance. Having this at the same level as the inner wall (being 0.80), it lowers the final propellant temperature to 920.4 K. Insulating the outer wall is thus a good way to increase the RAC efficiency.

Inputs			
Name	**Symbol**	**Value**	**Unit**
Tubing diameter	D_{tub}	0.002	m
Input power	P_{in}	1000	W
Absorption inner wall	α	0.90	-
Correction factor	a	0.023	-
Number of channels	m	8	-
Number of elements	n	100	-
Tubing length	L	0.10	m
Propellant	-	Nitrogen	-
Starting propellant temperature	$T_{p,0}$	298.15	K
Starting propellant pressure	p_p	$2.5 \cdot 10^5$	Pa
Universal gas constant	R_A	8.314	kg/K/mol
Total mass flow	mdot	$300 \cdot 10^{-6}$	kg/s
Conductivity RAC material (copper)	k_{RAC}	401	W/m/K
Conductivity propellant (nitrogen)	k_p	0.20	W/m/K
Emissivity inner wall	ϵ_1	0.80	-
Emissivity outer wall	ϵ_1	0.10	-
Enthalpy values propellant (nitrogen)	-	-	J/kg

Table 3.4: RAC tool: example inputs.

Outputs			
Name	**Symbol**	**Value**	**Unit**
Final propellant temperature	T_p	970.8	K
Heat exchanger efficiency	η	21.9	%
Propellant tubing loss	$p_{loss,tubing}$	1014.4	Pa

Table 3.5: RAC tool: example outputs.

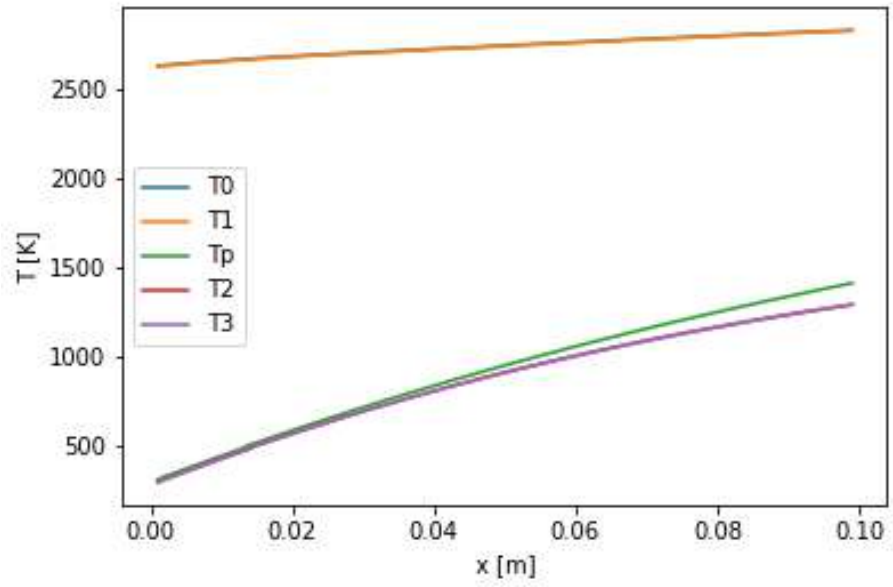

Figure 3.5: RAC tool temperatures output.

It was tried to use the tool developed by Leenders & Batenburg [43] to verify the outputs, but unfortunately it was not possible due to the fact that they require an input stating the temperature of the inert gas present in the heat exchanger cavity. This has a high impact, so not verification could be done here.

3.2.8. RAC tool recommendations

A few recommendations to further expand the tool are listed here.

1. Adjust the model so that longitudinal material heat transfer is taken into account.
2. Implement an RAC mass calculation.
3. Implement the dependency of the propellant thermal conductivity on the propellant temperature.
4. Implement the possible effect of a present inert gas in the RAC.
5. Implement the shape in the model, making sure that reflected and emitted radiation is caught again. For this, view factors will be used, as was done by Preijde [10].
6. Implement radial direction temperature difference for the propellant.

3.3. Nozzle & performance tool

The third and final tool section will describe the nozzle of the STP thruster and the resulting performance. Again it is based on the theory taught in the course Thermal Rocket Propulsion (TRP) [25]. The propellant gas is assumed to be an ”ideal gas” and the flow in the nozzle to be one-dimensional, isentropic and steady. The code can be found in Appendix A.

3.3.1. Nozzle & performance tool lay-out

In Figure 3.6, the flowchart of the tool is shown. It consists of variables (in rhomboids) and script parts (in squares).

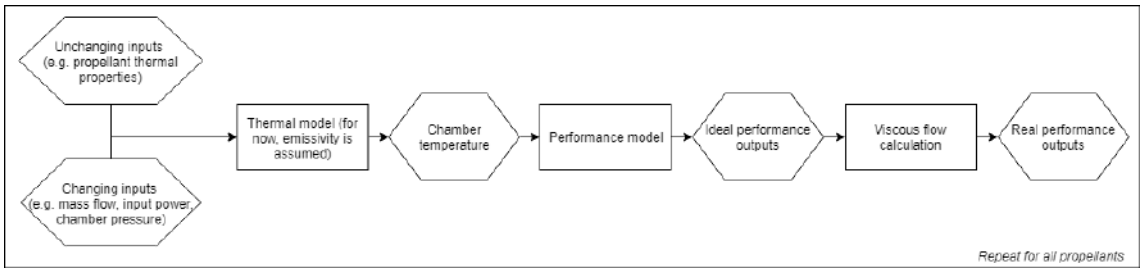

Figure 3.6: Flowchart of the tool.

Starting point is the heated propellant, of which T_p is known, now being called T_c. Then, the specific gas constant (R) and the specific heat coefficient (c_p) are calculated, giving way to the specific heat ratio (γ).

Because all these parameters are known, the throat area can be calculated using Equation 3.27, where Γ is the Vandenkerckhove function solely dependent on γ (see Equation 3.28).

$$A_t = \frac{\dot{m}_{ideal}\sqrt{R \cdot T_c}}{\Gamma \cdot p_c} \tag{3.27}$$

$$\Gamma = \sqrt{\gamma} \cdot \left(\frac{2}{\gamma+1}\right)^{\frac{\gamma+1}{2(\gamma-1)}} \tag{3.28}$$

The nozzle is assumed to be adapted to Sea Level (SL), which means that the ambient pressure p_a equals the exit pressure p_e. So, for SL:

$$p_e = p_a = 101\,325\ \text{Pa} \tag{3.29}$$

Because the chamber pressure is dictated by the feed system, the pressure ratio between chamber and nozzle exit is known. This pressure ratio is used to determine the area ratio via Equation 3.30, through which the exit area can be calculated (see Equation 3.31).

$$\frac{A_e}{A_t} = \frac{\Gamma}{\sqrt{\frac{2\gamma}{\gamma-1} \cdot \left(\frac{p_e}{p_c}\right)^{\left(\frac{2}{\gamma}\right)} \left(1 - \left(\frac{p_e}{p_c}\right)^{\left(\frac{\gamma-1}{\gamma}\right)}\right)}} \tag{3.30}$$

$$A_e = \frac{A_e}{A_t} \cdot A_t \tag{3.31}$$

Now, the equivalent velocity of the flow can be determined using Equations 3.32 and 3.33.

$$U_e = \sqrt{2 \cdot \frac{\gamma}{\gamma - 1} \cdot R \cdot T_c \cdot \left(1 - \left(\frac{p_e}{p_c}\right)^{\left(\frac{\gamma-1}{\gamma}\right)}\right)} \tag{3.32}$$

$$U_{eq} = U_e + \frac{p_e - p_a}{\dot{m}_{ideal}} \cdot A_e \tag{3.33}$$

Finally, the thrust (F), the I_{sp} and the characteristic velocity (c^*) can be calculated using Equations 3.34, 3.35 and 3.36.

$$F_{ideal} = \dot{m}_{ideal} \cdot U_{eq} \tag{3.34}$$

$$I_{sp,ideal} = \frac{U_{eq}}{g_0} \tag{3.35}$$

$$c^* = \frac{\sqrt{R \cdot T_c}}{\Gamma} \tag{3.36}$$

As can be seen, the thrust, specific impulse and mass flow all wear the subscript "ideal". Especially at low thrust levels (and thus mass flows), one should take care to use the assumption of inviscous flow. When the Reynolds number (see Equation 3.37) drops below 10 000, a laminar boundary layer occurs in the throat and a corresponding discharge coefficient discharge coefficient (C_d) will affect the mass flow according to Equation 3.38. Here, t stands for throat.

$$Re_t = \frac{4\dot{m}}{\pi D_t \mu_t} \tag{3.37}$$

$$C_d = \frac{\dot{m}_{real}}{\dot{m}_{ideal}} \tag{3.38}$$

In Figure 3.7, C_d as a function of the Reynolds number (Re) for various gases is shown [9]. Based on that, once Re is known, one can make a (somewhat accurate) prediction of the losses due to a boundary layer forming.

The throat dynamic viscosity (μ_t) is strongly dependent on the local temperature, which can be calculated via Equation 3.39, where the throat Mach number (M_t) equals 1 because the flow is assumed to be choked. For gases, Equation 3.40 shows how the dynamic viscosity might be calculated using Sutherland's formula [54]. For that equation:

- μ_t = viscosity in centipoise at input temperature T_t
- μ_0 = reference viscosity in centipoise at reference temperature
- T_t = input temperature in degrees Rankine
- T_0 = reference temperature in degrees Rankine
- C = Sutherland's constant

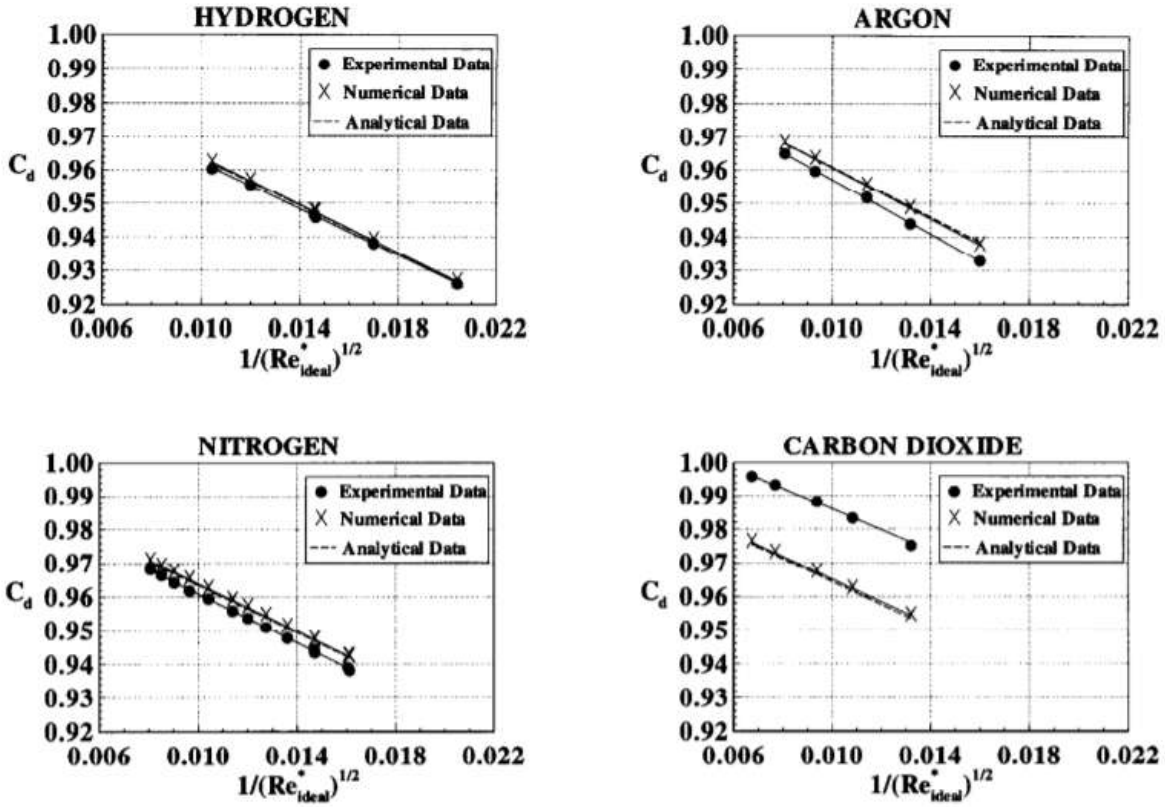

Figure 3.7: Discharge coefficient as a function of Reynolds number for various gases [9].

Alternatively, for water the dynamic viscosity is calculated using Equation 3.41 [55].

$$T_t = \left(1 + \frac{\gamma - 1}{2} M_t^2\right)^{-1} \cdot T_c \tag{3.39}$$

$$\mu_t = \mu_0 \left(\frac{T_0 + C}{T_t + C}\right)\left(\frac{T_t}{T_0}\right)^{\frac{3}{2}} \tag{3.40}$$

$$\mu_{t,water} = 2.414 \cdot 10^5 \cdot 10^{\left(\frac{247.8}{T_t - 140}\right)} \tag{3.41}$$

$$F_{real} = \dot{m}_{real} \cdot U_{eq} \tag{3.42}$$

Using all equations (3.37-3.42), one can calculate the real mass flow and its corresponding thrust level.

3.3.2. Nozzle & performance tool example calculation

The model constructed above was used to get a feeling of the values that could be achieved. Looking at the temperature and specific impulse values, it was seen that problems could be encountered with high specific impulse (>100 s). It would simply mean that the chamber temperature would also increase to

immensely high temperatures, in the range of several thousand Kelvins. Furthermore, a comparison between the different propellants could be made.

In Table 3.6, an example is shown, with inputs for nitrogen. Values for input power, mass flow and chamber pressure were chosen according to literature. The input power is not too high, as the choice for a heat-resistant RAC material is limited. The remaining inputs are from NIST ([50]) or assumed for now.

Inputs			
Name	**Abbreviation**	**Value**	**Unit**
Propellant temperature	T_p	970.8	K
Ideal mass flow	$\dot{m}_{ideal}$	300	mg/s
Chamber pressure	p_c	2.0	bar
Gravitational acceleration (SL)	g_0	9.81	m/s^2
Ambient pressure (SL)	p_a	101325	Pa
Universal gas constant	R_A	8.314	J/K/mol
Molar mass (nitrogen)	MM	28.0134	g/mol

Table 3.6: Example inputs

The outputs from the model are listed in Table 3.7. One can clearly see that the thrust is reduced by more than 5 percent due to the low throat Reynolds number (<10 000). Furthermore, as expected, the specific impulse is on the low side compared to the listed values from Leverone [11].

The program outputs the nozzle throat and exit area as well. These values are used in the thesis for dimensioning the nozzles. It should be noted that it is not yet known whether nozzles having these dimensions can be manufactured cheaply. That is an issue which should be looked into in the thesis.

Outputs			
Name	**Abbreviation**	**Value**	**Unit**
Specific impulse (SL)	I_{sp}	61.1	s
Reynolds number (throat)	Re_t	4896.3	-
Discharge coefficient (throat)	C_d	0.949	-
Ideal thrust (SL)	F_{ideal}	180.0	mN
Real thrust (SL)	F_{real}	170.7	mN

Table 3.7: Example outputs

Next to the nitrogen example, a comparison between the different propellants in graphs is outputted. The result is shown in Figure 3.8. Hydrogen is the best performing propellant when specific impulse and thrust are important, due to its low molar mass. However, the disadvantage is the poor storability; because of the low density, large volumes are needed.

The other three propellants perform about equally well at low input power values. Water lags behind though, due to the high amount of heat needed to vaporize.

3.3.3. Nozzle & performance tool recommendations

A few recommendations to further expand this section of the tool are listed here.

1. Incorporate the losses due to wall heat transfer, non-ideal gas behaviour and boundary layer.
2. Implement the option to input the nozzle shape and dimensions.

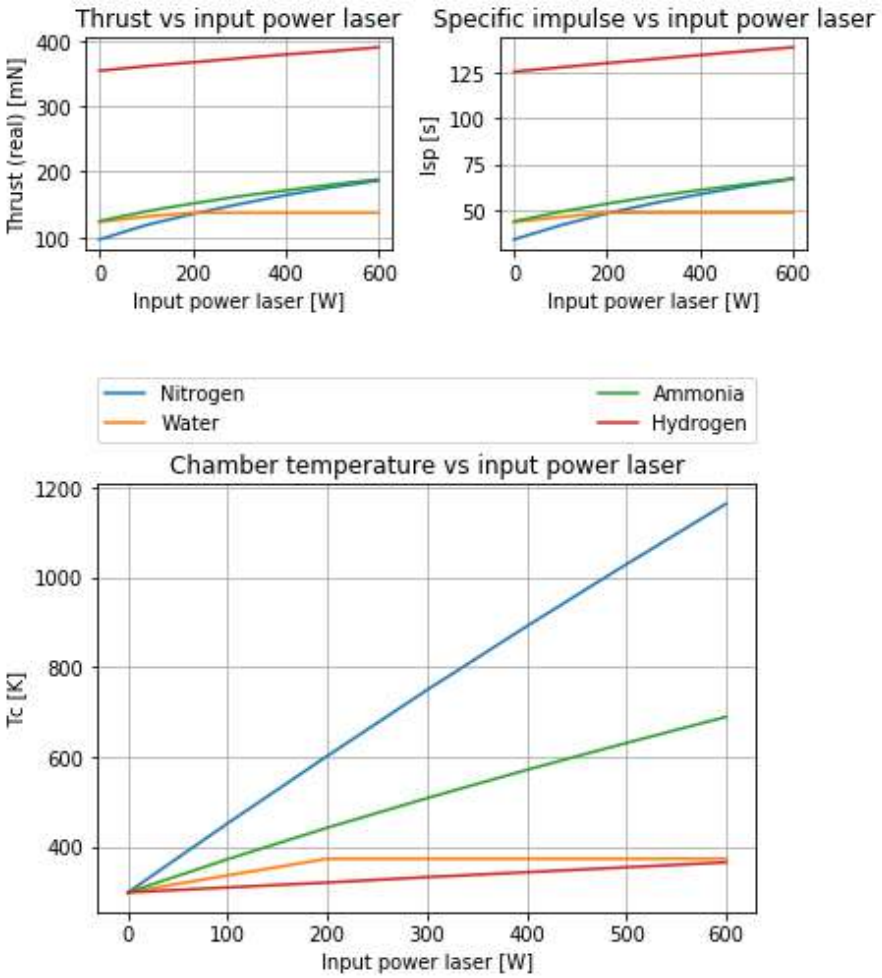

Figure 3.8: Output graphs from the model.

3.4. Tool summary

A few things can be concluded from this chapter:

1. Having the propellant in a liquid state will greatly decrease the propellant tank mass, because of the higher propellant density and thus lower tank volume. However, this likely brings the complexity of cryogenic storage (e.g. for hydrogen and ammonia), requiring measures to counter boil-off such as insulation or thermal control.
2. The heat exchanger is, for STP, the most crucial part of the thruster. Having a high efficiency in this segment can make the concept competitive with respect to other propulsion subsystems, such as chemical and electric propulsion. For this, especially the radiation losses should be minimized as far as possible. On the outside this requires some kind of insulation to lower the emissivity, on the inside it will require a material that has both high absorption and low emissivity, which are rare [56]. Likely some kind of paint needs to be applied on the side.
3. Assessing the heat exchanger efficiency is complex, as it is dependent on multiple variables, such as shape, configuration, tubing lay-out, material and so on. Not much literature goes in-depth on this issue and multiple assumptions often have to be taken to design an RAC.
4. The performance, especially the specific impulse, greatly depends on the chamber pressure, which in turn relies on the feed pressure and losses in RAC and tubing. Having a low chamber

pressure (Leenders employed 2 bars) will thus lower the specific impulse significantly.

5. It is difficult to show the accuracy of the model. In the above sections suggestions were given to enhance the tool, of which a not insignificant portion relates to the accuracy. The tool is thus mainly meant as aid in designing the RAC.

4

Data acquisition

The tool described in Chapter 3 needs to be validated in order to assess whether it outputs realistic data. For that, experimental data is needed. On the concept of STP, not much data is readily available in detail. Leenders of course did his experiment a decade ago [6], but the experiment lacked, mainly in performance (see Chapter 2). So, this chapter will describe what is needed to conduct another experiment in the field of STP, how this should be done and what is recommended through literature.

It should be noted that the experiments will not be done in vacuum. There is a vacuum oven available in the faculty of AE that can fit an STP microthruster, but it is too small to also hold the light source. If the vacuum chamber is used, it will result in added complexity if even possible. It is thus decided not to use this chamber and do the experiments at approximately sea level conditions, which are of course recorded using pressure and temperature sensors.

The chapter is divided into four distinct sections. First, the light source will be dealt with, followed by the sensors needed to retrieve useful data from the experiment. Then, the propellant is briefly described. In the end, the setup of the experiment, including a test plan, is discussed.

4.1. Light source

For the further course of the project, it is crucial to find a suitable heat source. If the result of this section is that no high-powered heat source can be found, the testing of the thruster will most likely not happen. If this is the case, what started as a practical study will turn towards a theoretical study, wherein most likely the performance model will be expanded towards a design model.

4.1.1. Light source requirements

In ground testing, it is practical to replace the concentrator system (see Section 2.1) by a light source that has a higher power flux than the Sun. It relaxes the number of components and focuses the experiment on other important aspects of the STP system, such as the heat exchanger. There are some requirements that need to be met by this light or heat source in STP testing:

1. The heat source needs to be high-powered. In literature, a concentrator system for smallsat applications can potentially deliver 100's of Watts [45]. In Leenders' experiments [6], around 60 Watts reached the heat exchanger, while the theater lamp has a listed power of 1000 W. A

minimum of 100 Watts is thus deemed necessary for the light source in order to have a possible experiment add value to the STP concept.

2. The heat source needs to be coherent. One should be able to measure or know what amount of power is outputted in a certain direction. A normal heater, which is found in housing, for instance has the disadvantage that it is harder to find out in what direction what amount of heat is dissipating.
3. The heat source needs to be controlled. Being able to control the amount of outputted power by the heat source makes the experiment more flexible.
4. The heat source's spectrum (in case of radiative heating) needs to resemble the Solar spectrum. Particularly in case of the heat exchanger, the spectrum is important as the absorption value is dependent on it. Having a high absorption for infrared light does not necessarily mean that a material or coating is suitable for solar irradiation usage.
5. The heat source needs to be easily available. Preferred is a heat source that can be borrowed at no cost, as resources for master theses are tight.

There are three types of light sources that are considered here: lasers, lamps and radiators.

First of all, the high-powered laser is assessed. Lasers emit continuous or pulsed light at one particular wavelength and have coherent (small) beams. In general (at the faculties at DUT), the lasers can be adjusted in power. The downside is the wavelength which does not resemble the solar spectrum, which could also make absorption harder and less realistic.

Another type of heat source that (nearly) fulfills the requirements, is high powered lamps. It was already seen at Leenders' thesis [6] that a theater lamp (1000 W) can be used to assess the feasibility of STP. However, because the real life solar input will be expected to be a multiple of the theater lamp power [45], lasers are preferred. Lamps also have the disadvantage of high attenuation (see Leenders again), but have the advantage to have a closer spectrum to the Sun with respect to lasers that operate on one specific wavelength.

What also could be used as a light source, are heat sources specifically meant for heating e.g. a room. There are radiators available that also can be adjusted in power. However, the downside which Leenders also encountered was the huge amount of loss towards the surroundings, making the actual power input to the heat exchanger difficult to quantify.

Considering the three descriptions above, it is decided to look for high-powered at the faculties of DUT. It should be noted that, in case no suitable lasers can be found, the project should make a turn. It could either accept a inferior heat source or turn its attention to a more theoretical study about STP. This chapter in large determines what road shall be taken.

4.1.2. High-powered laser options

A number of faculties at DUT employ lasers for various ends. However, the equipment is not listed somewhere and the responsible people need to be approached in order to retrieve characteristics and see if the heat source is available. Below, a list of options is given. Added to each item is considerations into the use of the heat source.

1. At the faculty of AE, at the Aerodynamics & Propulsion Laboratory, they employ lasers with pulsed shots for Particle Image Velocimetry. However, because it is not continuous according to assistant professor Dr. Ir. Ferry Schrijer, it only delivers a mean of 1 Watt, which will not be sufficient to power the thruster.

2. The department of Aerospace Structures & Materials owns a laser at their laboratory. According to technician Frans Oostrum, contact persons are assistant professor Dr. Roger Groves and researcher Dr. Andrei Anisimov. They replied that there are three powerful lasers available:
    - The Sirius laser facility (https://tinyurl.com/y6zqnmqo) is a pulsed laser (400 Hz) at about 600 mJ per pulse, which totals to approximately 240 W. The wavelength of the laser is 308 nm, which is in the UV part of the spectrum. Further questions were to be asked to Dr. Anisimov and PhD candidate Dmitrii Kliukin.
    - The Innolas Spitlight 600 (https://tinyurl.com/y6gtysfz) has pulses at 700-800 mJ at 1064 nm or 400-500 mJ at 532 nm. The frequency is 10 Hz, so only has a maximum of 10 W, which is too low to be used as a heat source for this project.
    - The Philips VCSEL PPM412-12-980-24 (https://tinyurl.com/yyosnpcw) is utilized for the heating of composites. It has a power output of 2.4 kW and the contact person is assistant professor Dr. Ir. Julie Teuwen.
3. The Faculty of Applied Physics (TNW) employs lasers but the test facility is unfortunately too small for the engine to be tested.
4. At the department of Chemical Engineering (TNW "Zuid") they also employ lasers. Unfortunately, they are too low-powered to be of use. Contact persons were technicians Christiaan Schinkel and Jos Thieme.
5. The faculty of Industrial Design responded that no lasers are available for this kind of research.
6. It was advised to visit the website www.materialsequipment.4tu.nl, but it turned out that this website is far from complete and does not show any necessary specifications.
7. At the faculty of Faculty of Mechanical, Maritime and Materials Engineering (3mE), at the department of Materials Science and Engineering, they employ a Nd:YAG laser primarily used for welding research. The laser has just been replaced and will be operational from March 2019 on. Welding technician Jurriaan van Slingerland was the first to go to, professor Dr. Ian Richardson is officially in charge. The laser has a power from 50 W to 8000 W and can be set at 1 W accuracy.

4.1.3. Light source choice

Looking at the listed options in Section 4.1.2, it can be seen that options 2 and 7 are promising as they provide enough power (above 100 Watts). It was arbitrarily chosen to enquire to see if number 7 was available. After a meeting with Van Slingerland and some email conversations, professor Richardson gave his approval of the test. Conditions are that Mr. Van Slingerland approves the experiments, safety is guaranteed and that the technician is mentioned in the appropriate papers.

The wavelength of this laser is 1064 nm, which lies in the infrared part of the spectrum. In the focal point of the laser, the beam has a diameter of 0.20 mm. Because the welding table can be adjusted in height, the laser beam can also be defocused to a maximum of (at least) 50 mm width.

4.1.4. Light source conclusion

It was important to assess whether suitable light sources were available for the experimental phase of the thesis. A light source is deemed suitable when it can reach power levels above 100 Watts, has low losses, high coherence, high controllability and a similar spectrum to the Sun. For now, the welding laser at the faculty of 3mE is identified as a possible option for the testing and it was already enquired whether it is allowed to use, which it is.

4.2. Equipment

For data acquisition in experiments, equipment such as sensors are needed. In the subsections below, first the Meetshop will be explained, after which the used software and the four sensor types are described. In the end, there is a small subsection on the available cameras.

What becomes clear after searching literature is that no documented testing was done in the area of STP in the last decade, after Leenders did his experiments in 2008. As inputs for the section below are thus experiments which were already described by Leenders in his thesis ([6], Chapter 7). In general, test results are described quite extensively, but the means to get to this data (what sensors, what range, what accuracy) unfortunately are not.

4.2.1. Meetshop

Because the bulk of the experiments will not be done at the faculty at AE, where all equipment is available, multiple sensors need to be found and elaborated on. The Meetshop, located at the faculty of 3mE is of use here. The manager, Jos van Driel, has all sorts of electrical equipment and data acquisition systems. A large array of sensors and Data Acquisition (DAQ) devices can be borrowed at this shop. Furthermore, he is able to assist with data acquiring through Laboratory Virtual Instrument Engineering Workbench (LabVIEW), see next subsection.

He has, among others, at least four thermocouples and two pressure sensors available that can be attached to DAQ devices that in turn can be connected to a pc/laptop. He does not have mass flow sensors available. Normally one can borrow the sensors for three weeks, but six weeks is possible. From the end of April until June it could be that he is too busy to help out.

4.2.2. LabVIEW

To handle the output of the sensors, LabVIEW is used. It is a software program, developed by National Instruments (NI), which visualizes the data and eases the process of data handling and saving. It was recommended by Van Driel because of its availability at DUT, its ease of use and large range of options. Leenders also used LabVIEW for his experiments. Van Driel suggested to download the 2018 version from software.tudelft.nl.

In Figure 4.1, a LabVIEW Instrument (or script) is shown. On the right, the front panel or end is shown. That is what the user will eventually see. On the left is the back end, which is also called ”the block diagram”, because it indeed features blocks. Altering something in one of the windows also has its effects on the other.

For this project, a script was made which takes the input of various sensors (see sections below) and translates them to a text (.lvm) file. The file can be opened by Excel and then modified further. Simultaneously, the input of the sensors is shown in waveform graphs, so the test can be followed in real time.

4.2.3. Temperature

The sensors need to measure the temperature at various locations, including at multiple spots at the outside and inside of the RAC and (if possible) at the beginning and end of the nozzle. Thermocouples seem to be a good choice, because of their low cost and easy use, while still being fairly accurate (with a deviance up to 10 deg. C [57]). Leenders does not comment on the needed accuracy, but reports similar values. It is expected that a maximum deviance of 10 deg C is sufficient, as the temperatures of propellant and RAC will likely surpass the 1000 K mark.

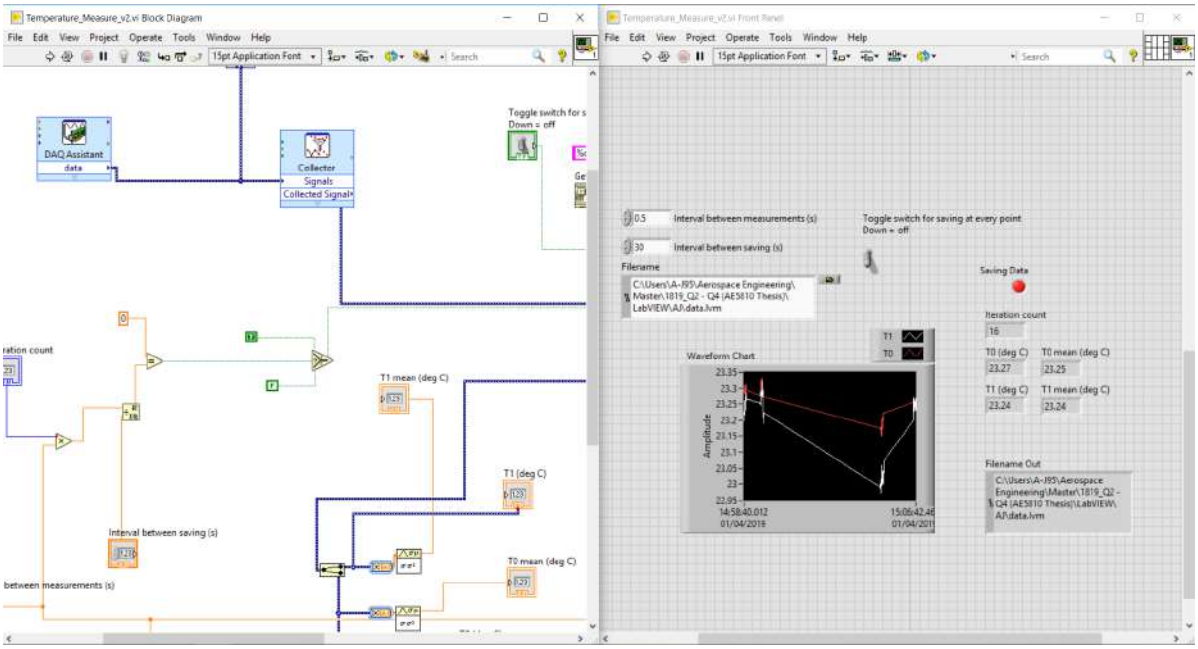

Figure 4.1: LabVIEW example

Thermocouples can be borrowed from the Meetshop at the faculty of 3mE. They can be connected to a small device which in turn can be connected to a computer, where the data can be accessed via LabView. There are six thermocouples available, which are connected to National Instruments (NI) DAQ devices. Type K thermocouples available at the Meetshop have a maximum temperature of 750 degrees C or 1023 K (https://tinyurl.com/y27ab8pz). Higher temperature thermocouples (type N), which measure a maximum temperature of 1300 degrees C or 1573 K, can be bought at https://tinyurl.com/y2txhjb3. Both thermocouples have the advantage of being fully isolated, making them invulnerable to short circuiting. However, if they have to be bought, they tend to be expensive (about €40,- each). In Figure 4.2, the NI 9211 DAQ and two thermocouples (the silver one having a maximum temperature of 1573 K, the other one 673 K) are shown. These devices can hold up to four thermocouples, multiple devices can be connected to a pc or laptop. The maximum frequency of measurements is about 2 Hz, which will be sufficient because the tests will have a duration of multiple minutes.

It is expected that the temperature sensors will be mounted in the propellant inlet tube (or on the outside wall of the tube), the nozzle wall, at the beginning of the RAC (outer wall and inner wall) and at the end of the RAC (outer and inner wall). That way, the tool developed in Chapter 3 can be validated using the temperatures outputted by the sensor. The propellant inlet thermocouple is important because it can assess the propellant inlet temperature, necessary to calculate the resulting performance (in terms of thrust and specific impulse). It should be noted that the thermocouples, as shown above, have a maximum temperature. It could be possible that they can thus not be mounted on the RAC inner wall, as the light source will illuminate that part, destroying the sensors in the process. Leenders mounted six thermocouples on the heat exchanger and nozzle, four of them on the RAC outer wall [6]. Three of those are on one side at equal spacing, the other is opposite from the first one. The last two of the six are at the propellant inlet and the inside nozzle.

In Figure 4.3, the output from the temperature sensors in LabVIEW is shown. The output is quite close to each other.

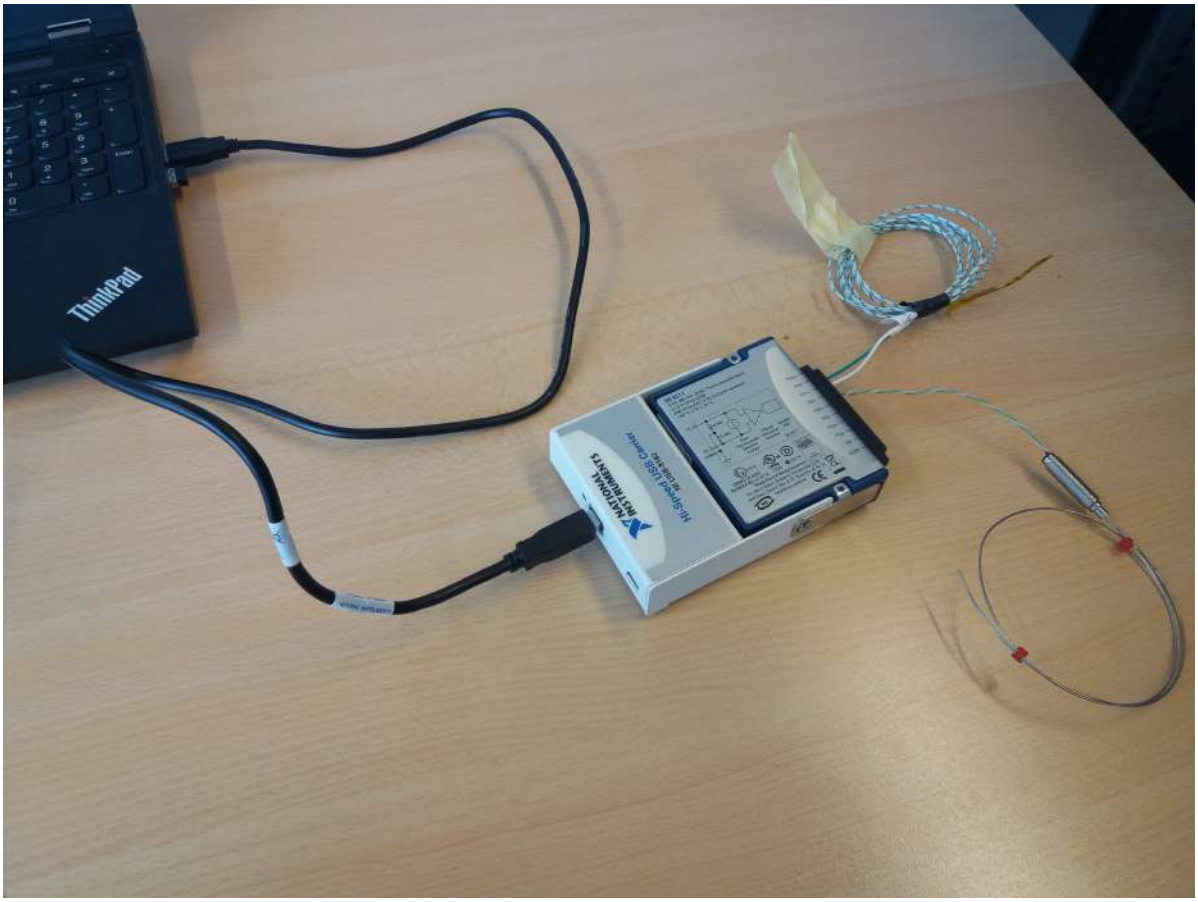

Figure 4.2: The NI 9211 DAQ and two thermocouples (the silver one having a maximum temperature of 1573 K, the other one 673 K).

4.2.4. Pressure

The pressure will be monitored by pressure sensors, which will also be borrowed from the Meetshop. They can be connected to a NI device which in turn can be connected to a computer, where the data can be accessed via LabVIEW. Because the sensors can only handle a maximum temperature flow of around 70 deg C, the sensors will most likely have a long tube connected to the system, in order for the flow to cool down. This will make the setup more complex, which will probably result in only two pressure sensors at most, at the inflow manifold of the RAC and at the end of the nozzle. Leenders [6] had them at the same locations.

The first pressure sensor (called "pressure_0") that is now available is the pressure transmitter DRTR-AL-20MA-R16B, which measures an over-pressure of 0-16 bar, corresponding to 4-20 mA. Through the use of a 558 Ohm resistor, the voltage can be read and translated to a pressure. The sensor must be connected to the grid (230 V). It is reported to have an accuracy of 0.2% [58], which is again similar to Leenders' listed values.

The second pressure sensor (called "pressure_1") available is the DRTR-ED-10V-A10B, which measures an absolute pressure of 0-10 bar, corresponding to 0-10 V. No resistor is required as the output is already a voltage. The sensor must also be connected to the grid (230 V).

In Figure 4.4, both pressure sensors are shown, connected to a laptop via a NI device (6008 USB). The sensor with the blue tube measures the over-pressure up to 16 bar. In Figure 4.5, the output from the pressure sensors in LabVIEW is shown. There is quite some discrepancy between the sensors, which should measure ambient pressure (about 1.01 bar). This should be further investigated in the

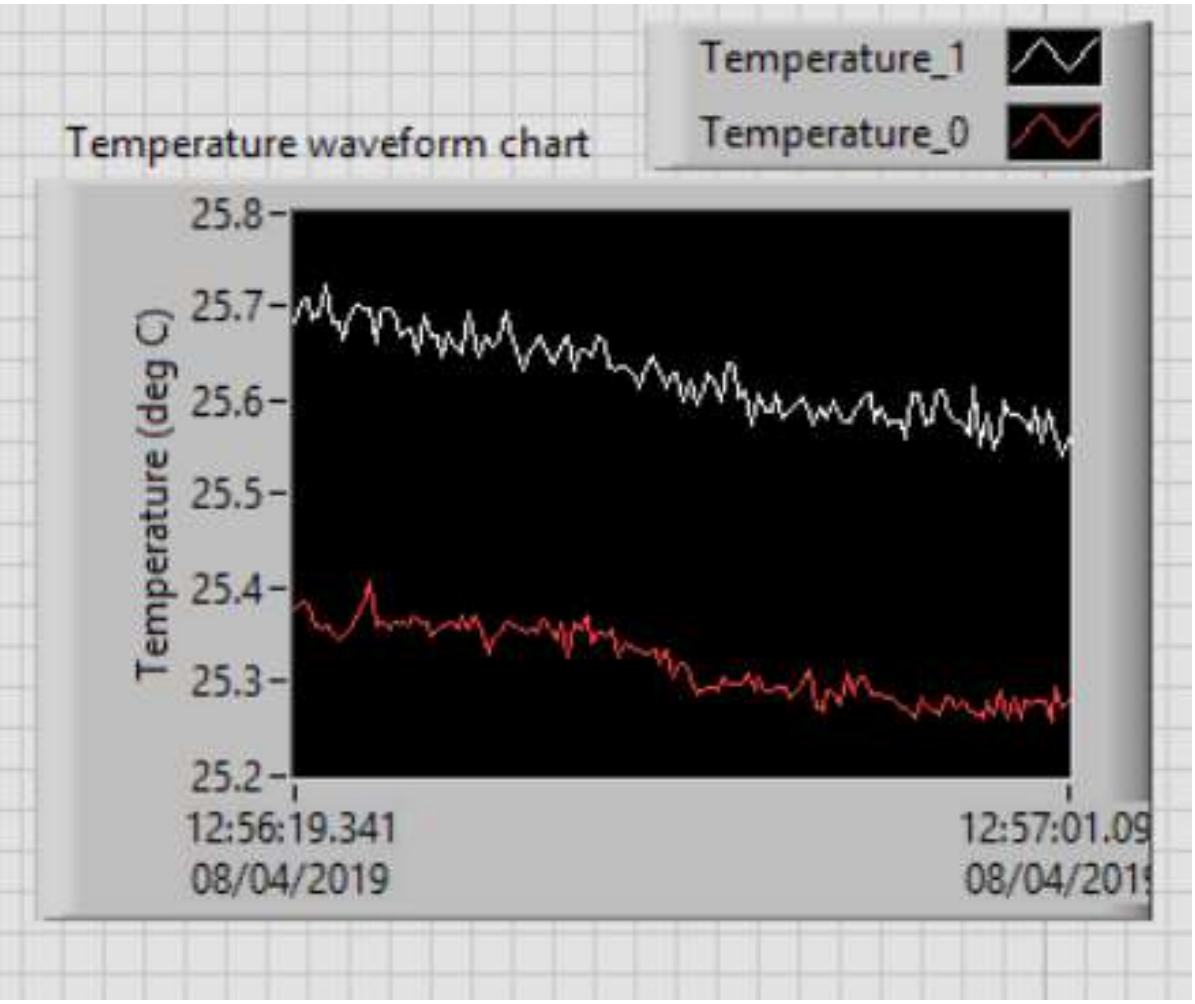

Figure 4.3: LabVIEW output for the temperature sensors.

thesis.

4.2.5. Thrust

The thrust will be measured via a sensor embedded in a thrust bench. This trust bench is the TB-1.1, developed at the faculty of AE by a master student in 2007 for the purpose of testing microthrusters [59]. The bench has dimensions of $61 \times 34 \times 22$ cm^3 and a total mass of 3.17 kg, where the inner frame is 1.64 kg and the outer frame is 1.53 kg. The working range is from 50 to 1000 mN with an accuracy of 10 mN. See Figure 4.6 for the thrust bench. The accuracy that can be distilled from result graphs from Leenders is also around 10 mN. It it thus deemed accurate enough.

The thrust sensor itself is a FUTEK LSB200 sensor, with an RS232 connection. To connect it to a pc or laptop, a USB to serial device was first used. LabVIEW did recognize the input, but it could not acquire any data. So it was decided to look up the wiring diagram and connect the four wires directly to the same NI device measuring the pressure (NI USB-6008 device). This turned out to yield results, but because of the low voltages (in the range of a few millivolts), an amplifier was added which boosted up the voltage signal to several volts. Added to that, the amplifier houses potentiometers which can tweak the ”rest signal” to zero.

It should be noted that another load sensor is available, the FUTEK LRF400 with a maximum load

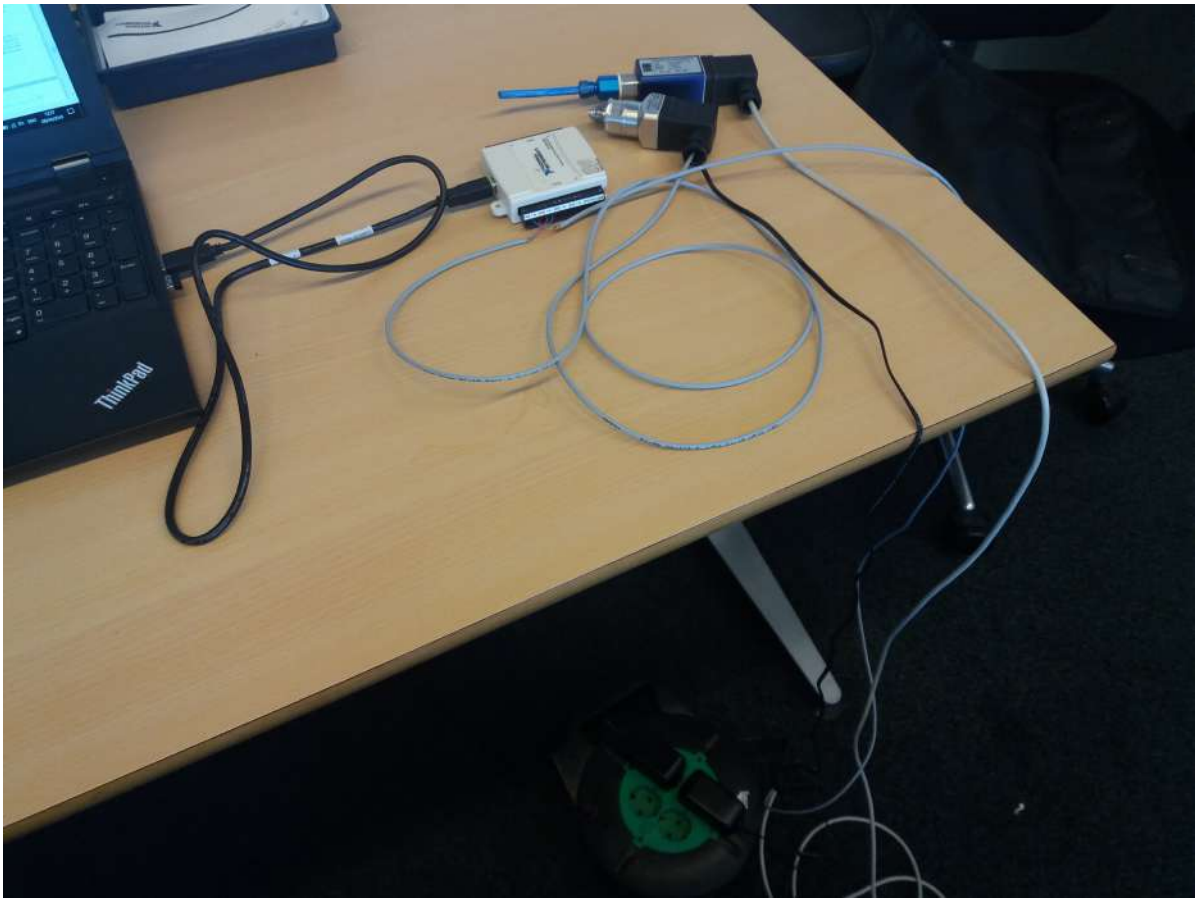

Figure 4.4: The NI 6008 USB and two pressure sensors (the one with the blue tube being the 16 bar one).

range of 100 mN. It is more accurate than the LSB200 variant. It has to be investigated in the thesis what sensor is most useful in the test setup.

4.2.6. Mass flow

In order to validate the model results for performance of the thruster, the mass flow should be monitored. However, the mass flow is a hard thing to measure. Mass flow sensors are often very specialized in that they only measure a specific interval of a specific fluid or gas. They do not have mass flow sensors at the Meetshop available, but they are present in the cleanroom of the Space Systems Engineering chair at the faculty of AE.

There are three mass flow sensors available:

1. Brooks 5850S Smart Mass Flow. Range from 0-144 mln/min of nitrogen, or 0-3.00 mg/s.
2. Brooks 5850S Smart Mass Flow. Range from 0-2 ln/min of nitrogen, or 0-41.69 mg/s.
3. Brooks 5851S Smart Mass Flow. Range from 0-47.3 ln/min of nitrogen, or 0-860.83 mg/s.

The units ”mln” (milliliter normal) and ”ln” (liter normal) refer to the fact that the volumetric flow is measured at normal conditions, which corresponds to a temperature of 0 deg C and 1 atm (Brooks manual [60]). The density of nitrogen gas at these properties equals 1.2506 kg/m^3 [61], thus giving the mass flow values stated above. The accuracy is listed at 0.5% of the maximum rate.

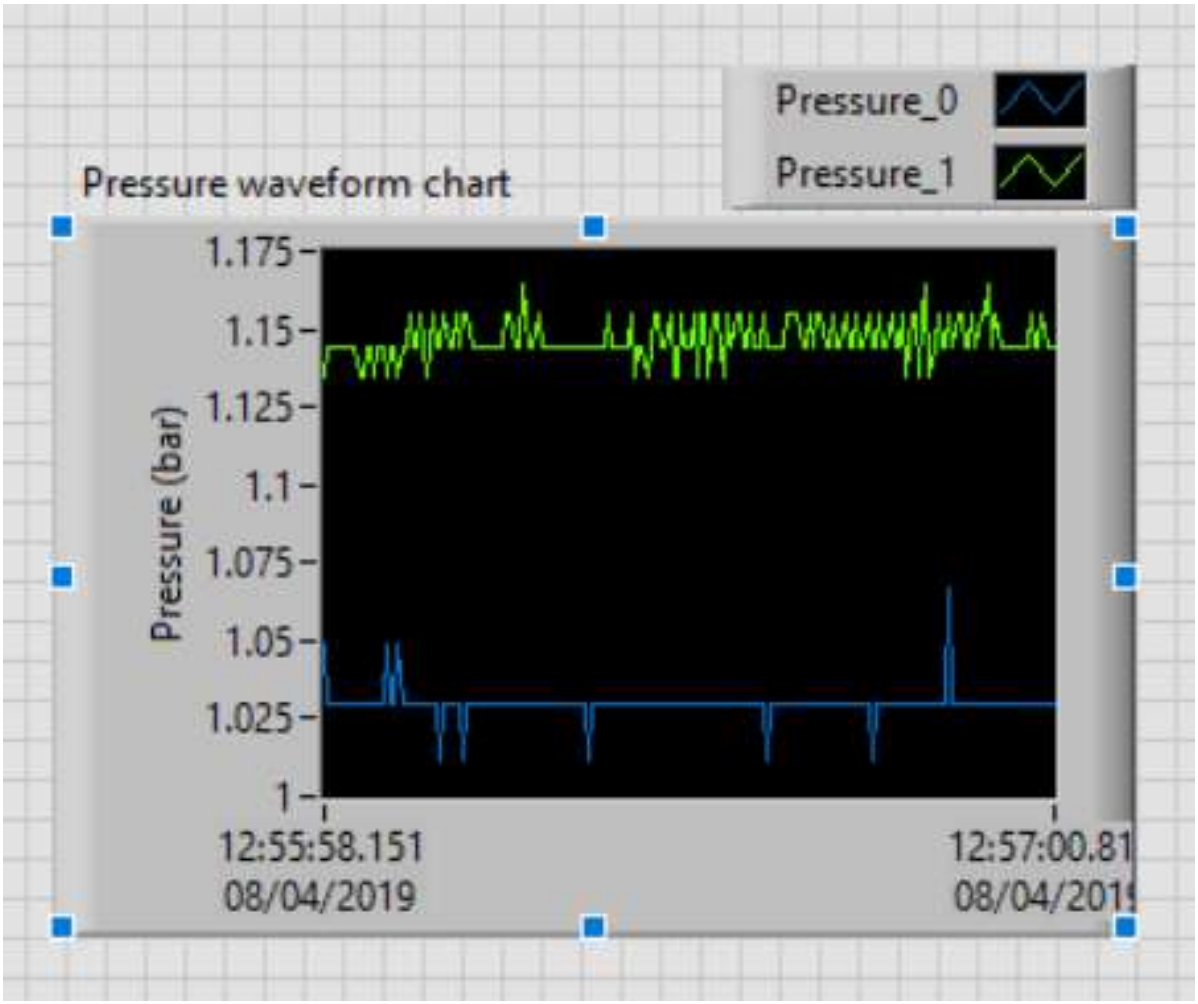

Figure 4.5: LabVIEW output for the pressure sensors.

Leenders employed a mass flow of around 300 mg/s. Looking at the mass flow ranges listed, the third sensor (see Figure 4.7) is the only sensor capable of measuring those mass flows and will thus be chosen.

The third sensor has not been calibrated in the last decade, however the two lower range sensors (the 5850s) have. It turned out that this has but a small effect on the accuracy for these two. For now it is decided not to calibrate the 5851 sensor, but check its validity against data already generated in Leenders' thesis. Next to that, the mass flow sensors can be compared to each other to get a feeling of their accuracy.

It should be noted that, according to the Brooks manual [60], the mass flow sensors become more inaccurate at lower mass flow ranges, lower than 20% of the full range. Care should be taken to stay outside of this region.

4.2.7. Power meter

It is believed that a laser, because of the coherent bundle and short distance, does not experience a lot of attenuation. However, a pocket meter (the PocketMonitor (PMT) 70iCu)is available at the lab (see Figure 4.8). The power meter can be positioned under the laser optical head to measure the power output of the laser at various instances, which could be used to calibrate the laser. It should be noted

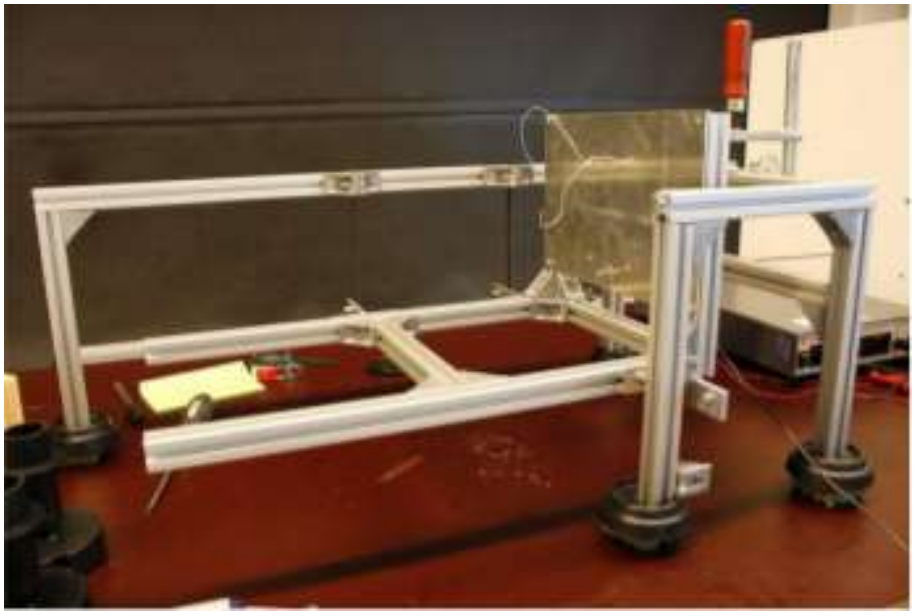

Figure 4.6: Thrust bench TB1-1 and FUTEK LSB200 force sensor.

that the maximum width of the "measuring cone" inside the power meter is about 25 mm, which holds that the beam cannot be defocused too much. At https://tinyurl.com/y345wofu, the manual can be found. The accuracy is within 4%.

4.3. Propellant

In Section 2.5 it was seen that gaseous nitrogen will most likely be used for experimenting, due to its non-toxic and non-corroding characteristics and high availability. Pressurized nitrogen cylinders can be delivered to the laser facility by the "Gassenteam" ("Gas team") from DUT, located at Logistiek & Milieu. They have a contact with Van Slingerland, so the gas cylinder can be delivered directly to the welding facility.

4.4. Experiment setup

In this section, the experiment setup will be shown. More information about the setup can be found in Appendix B, where the test plan which was approved by Van Slingerland is located. Please note that this test plan is written as a stand-alone document, having amongst else an introduction to the concept of STP.

Leenders conducted three separate experiments, which included a dry test (without mass flow, with illumination), a test with propellant flowing while illuminated and a power flux measurement [6]. The first two ran for about two hours each, the third one for ten minutes. He did the testing on two separate days. Looking at these numbers, it is expected that doing all the experiments will cost about five to six hours in total, including the setup.

It is expected that this will not be significantly different in the experiments that are still to come for this thesis. Again, a power flux measurement will be done to validate the power input in the heat exchanger and of course an experiment with running propellant while illuminated will be conducted. The third experiment will be quite different, as it will have the propellant running without being heated, to see the performance difference between this and the second experiment.

Figure 4.7: Brooks 5851S Smart Mass Flow. Range from 0-47.3 ln/min of nitrogen, or 0-860.83 mg/s.

It should be noted that there is the advantage that tests without the light source are more flexible locationwise. Instead of using the welding facility this can be done in the cleanroom, located at the eight floor of the faculty of AE, where no technician is needed whatsoever. For the other two tests (firing while illuminated and power measurement), the facility will be needed. For the two experiments in the welding facility, the time needed is estimated at four hours. If possible, a second session of four hours will be planned a few weeks later to redo any tests which require so. The time is probably available, but is should be closely discussed with Van Slingerland.

In Figure 4.9, the bench and welding laser inside the laser facility are shown. In the foreground the (disconnected) optical head (see also Figure 4.10) is shown, in the background the moving rails can be seen. The rails will not be used for the experiment, there are useful to welders to execute a weld. The test bench should be secured to the table in some way. The ambient pressure and temperature have to be taken, the sensors required to do so should be brought.

When the STP thruster is designed, further elaboration can be given on the test setup.

Figure 4.8: The PocketMonitor (PMT) 70iCu power meter.

Figure 4.9: The welding laser and bench inside the laser facility.

Figure 4.10: The optical head of the welding laser, not connected to the bench.

5

Conclusions & recommendations

This chapter will describe the conclusions, followed by the recommendations. The final proposal for the thesis will be presented as a separate document.

5.1. Conclusions

The concept of STP has been researched extensively for the last few decades, both theoretically and practically. What becomes apparent from this research is that the propulsion concept has an advantageous I_{sp} with respect to chemical propulsion while still maintaining a medium level thrust, making it suitable for certain mission types such as orbit elevation. Furthermore, what is seen is that STP faces challenges in the concentrator components, collection of solar illumination and attitude fixation. The latter two can be mitigated using heat storage units and fiber optic cables respectively, with the disadvantage of added complexity.

For now, STP remains a concept which has never been flown in space. What is interesting is that it is stated that the propulsion option would benefit from laboratory-based studies, proving that the performance (in terms of specific impulse and thrust) can really be reached. In other words, a validation of the performance is needed. Because of that, literature towards data acquisition, including equipment, light source and software, was found. This was accompanied by a test plan. At first glance, having a suitable light source in the form of a welding laser, the experiments can be conducted.

The data to be validated will come from a tool developed to assess the performance of a designed STP thruster, called the STP tool. It will take in various parameters to predict temperatures, pressure, specific impulse and thrust of the motor. This tool is based on the scripts from Leenders. Please note that the script can be enhanced, see Chapter 3 for that.

As mentioned extensively in this report, Leenders conducted his research in the same experiment-based area as this will. It is thus wise to look into his work and use the recommendations he provides. One of these was to improve the light source, in terms of power that reaches the heat exchanger itself. It is an interesting notion, as various researchers also wrote down that hundreds of Watts will be needed to make the concept competitive. Next to that, changing the lay-out of the channels in the heat exchanger was recommended by Leenders. Because resources will be tight, this needs to be closely discussed with the manufacturer of the motor to see if it is feasible. Again, having a spiral tubing instead of a linear one is also recommended by other, according to Chapter 2.

Looking at the above, an outline already forms for the thesis. Please note that it is discussed more

elaborately in the proposal concurrent to this document. The rough outline for the coming months will be:

1. Extend the performance tool, especially regarding view factors. These enhancements will be based on the work Preijde did in his thesis [10].
2. Design the STT2 using the knowledge gained from this literature study. This is closely concurrent with the next step, being the manufacturing, and the tool developed before to reach optimum performance. It is no use to design a motor which cannot be made within the resources provided.
3. Manufacture STT2. This will be done within the environment of DUT and, as said before, closely related to the design step.
4. Predict motor performance, including I_{sp}, thrust, temperature and pressure.
5. Setup experiments.
6. Conduct experiments.
7. Analyse data.
8. Conclude on the feasibility of STP and provide recommendations.

5.2. Recommendations

Having stated the conclusions of this report, there are still some recommendations left for this work. First of all, there are numerous recommendations stated in Chapter 3, which reflect on the shortcomings of the performance tool as it is. The most primary one, as noted in the numeration above, is incorporating view factors. Next to that, no concentrator system is incorporated in the tool as it is obsolete when using the welding laser, which is already a focused large power source. Furthermore, because of time constraints, no research is done towards the manufacturability of the motor, especially on the heat exchanger and nozzle components.

Bibliography

[1] M. F. McKay, D. S. McKay, and M. B. Duke, *Space Resources - Energy, Power and Transport* (NASA, 1992).

[2] A. Takken, *Project Proposal and Plan*, Tech. Rep. (TU Delft, 2019).

[3] E. Kulu, www.nanosats.eu, *Nanosatellite Database,* (2018).

[4] Unknown, https://mech-hm.eng.hokudai.ac.jp/~spacesystem/images/Schematic_of_solar_thermal_propulsion.JPG, *STP schematic,* (2018).

[5] K. A. Ehricke, *The solar-powered space ship,* Convair Astronautics (1956).

[6] H. C. M. Leenders, *Development of a solar thermal propulsion system*, Tech. Rep. (TU Delft, 2008).

[7] J. M. Shoji, *Solar Rocket Component Study*, Tech. Rep. (Rockwell International, Canoga Park, 1985).

[8] P. N. Clark, J.-l. Desplat, H. H. Streckert, S. F. Adams, J. W. Smith, P. N. Clark, J.-l. Desplat, H. H. Streckert, S. F. Adams, and J. W. Smith, *Solar Thermionic Test in a Thermal Receiver,* in *AIP Conference Proceedings* (2006).

[9] A. N. Johnson, P. I. Espina, G. E. Mattingly, and C. L. Merklet, *Numerical characterization of the discharge coefficient in critical nozzles*, Tech. Rep. (University of Tennessee Space Institute, 1998).

[10] J. J. Preijde, *Design of a Solar Thermal Power-Propulsion System for a Small Satellite*, Tech. Rep. January (TU Delft, 2015).

[11] F. Leverone, A. Cervone, and E. Gill, *Cost analysis of solar thermal propulsion systems for microsatellite applications,* Acta Astronautica **155**, 90 (2019).

[12] P. Frye, *Integrated solar upper stage (ISUS) space demonstration design,* in *AIP* (1997).

[13] C. T. Kudija and P. E. Frye, *Integrated Solar Upper Stage (ISUS) engine ground demonstration (EGD),* in *AIP* (1998).

[14] C. C. Selph, *The place of solar thermal rockets in space,* AFRPL (1962).

[15] M. R. Gilpin, D. B. Scharfe, A. P. Pancotti, and M. P. Young, *Molten Boron Phase-Change Thermal Energy Storage to,* in *Distribution*, 0704 (2011) pp. 1–18.

[16] J. C. Mankins, *Technology Readiness Levels,* White Paper (April) Advanced Concepts Office. Office of Space Access and Technology. NASA. , 5 (1995), arXiv:arXiv:1011.1669v3 .

[17] P. Henshall and P. Palmer, *Solar Thermal Propulsion Augmented with Fiber Optics: - Technology Development,* in *42nd AIAA/ASME/SAE/ASEE Joint Propulsion Conference & Exhibit*, July (2006) pp. 1–12.

[18] P. Henshall, P. Palmer, and A. Baker, *Solar Thermal Propulsion Augmented with Fibre Optics: A System Design Proposal,* 41st AIAA/ASME/SAE/ASEE Joint Propulsion Conference & Exhibit , 1 (2005).

[19] K. Das, *Design and Thermal Analysis of a Solar Thermal Thruster*, Tech. Rep. (TU Delft, 2018).

[20] T. Nakamura, R. Krech, J. McClanahan, J. Shoji, R. Partch, and S. Quinn, *Solar Thermal Propulsion for Small Spacecraft - Engineering System Development and Evaluation,* in *41st AIAA/ASME/SAE/ASEE Joint Propulsion Conference & Exhibit* (2005).

[21] A. Janssens, *Solar Thermal Propulsion module for the Delfi-C3 nanosatellite: Design of a technology demonstrator*, Tech. Rep. (TU Delft, 2007).

[22] D. B. Scharfe and A. D. Ketsdever, *A Review of High Thrust , High Delta-V Options for Microsatellite Missions,* in *45th AIAA/ASME/SAE/ASEE Joint Propulsion Conference*, August (2009) pp. 1–14.

[23] H. C. M. Leenders, *Solar thermal propulsion Literature study*, Tech. Rep. (TU Delft, 2007).

[24] J. P. Carroll, R. Propulsion, L. Beach, and J. P. Carroll, *Solar Orbit Transfer Vehicle,* in *48th AIAA/ASME/SAE/ASEE Joint Propulsion Conference* (2000).

[25] B. Zandbergen, *AE4S01 Thermal Rocket Propulsion reader (version 2.06)*, August (TU Delft, 2017).

[26] J. M. Shoji, *Performance potential of advanced solar thermal propulsion,* in *AIAA* (1983).

[27] R. M. Zubrin and T. K. Sulmeisters, *The integrated power and propulsion stage: A mission driven solution utilizing thermionic technology,* in *AIP* (1992).

[28] J. D. M. Malloy, R. F. Rochow, and J. B. Inman, *Hybrid solar rocket utilizing thermal storage for propulsion and electrical power,* (1994).

[29] F. G. Kennedy and P. L. Palmer, *Preliminary design of a micro-scale solar thermal propulsion system,* in *38th AIAA/ASME/SAE/ASEE Joint Propulsion Conference & Exhibit*, July (2002) pp. 1–11.

[30] M. R. Gilpin, D. B. Scharfey, M. P. Youngz, and R. N. Webbx, *Experimental investigation of latent heat thermal energy storage for bi-modal solar thermal propulsion,* 12th International Energy Conversion Engineering Conference, IECEC 2014 , 1 (2014).

[31] M. R. Gilpin, *Phase-Change Thermal Energy Storage and Conversion : Development and Analysis for Solar Thermal Propulsion,* in *48th AIAA/ASME/SAE/ASEE Joint Propulsion Conference*, August (2012) pp. 1–11.

[32] F. Leverone, A. Cervone, M. Pini, E. Gill, and P. Colonna, *Feasibility of an Integrated Solar Thermal Power and Propulsion System for Small Satellites,* IAC (2017).

[33] F. Kennedy, P. Palmer, and M. Paul, *Results of a Microscale Solar Thermal Engine Ground Test Campaign at the Surrey Space Centre,* in *40th AIAA/ASME/SAE/ASEE Joint Propulsion Conference and Exhibit*, July (2004) pp. 1–11.

[34] F. G. Kennedy, *Solar Thermal Propulsion for Microsatellite Manoeuvring*, Tech. Rep. (University of Surrey, Surrey, 2004).

[35] H. Sahara and M. Shimizu, *Solar Thermal Propulsion System for Microsatellites Orbit Transferring,* in *40th AIAA/ASME/SAE/ASEE Joint Propulsion Conference and Exhibit*, July (2004) pp. 1–7.

[36] T. Nakamura, D. Sullivan, J. A. Mcclanahan, J. M. Shoji, R. Partch, and S. Quinn, *Solar Thermal Propulsion for Small Spacecraft,* (2004) pp. 1–11.

[37] H. Sahara, M. Shimizu, K. Osa, K. Watanabe, and Y. Nakamura, *Solar Thermal Propulsion for Microsatellites End-of-Life De-Orbiting,* (2003) pp. 1–8.

[38] M. Dhanasar, W. Edmonson, F. Ferguson, and I. M. Blankson, *Small Satellite Solar Thermal Propulsion System Design: An Engineering Model,* in *SpaceOps 2014 Conference* (2014).

[39] A. R. Tummala, *An Overview of Cube-Satellite Propulsion Technologies and Trends,* Aerospace **4**, 58 (2017).

[40] B. Y. Xing, M. C. Huang, M. S. Cheng, and K. Liu, *Influence of Thermal Decomposition of Ammonia Propellant in Solar Thermal Propulsion,* Applied Mechanics and Materials **598**, 257 (2014).

[41] S. Rabade, N. Barba, G. Liu, L. A. Garvie, and J. Thangavelautham, *The Case for Solar Thermal Steam Propulsion System for Interplanetary Travel: Enabling Simplified ISRU Utilizing NEOs and Small Bodies,* (2016) pp. 26–30.

[42] H. Leenders and B. Zandbergen, *Development of a Solar Thermal Thruster System,* 59th International Astronautical Congress , 1 (2008).

[43] H. C. M. Leenders and P. Batenburg, *Thermal control of a solar thermal propulsion system*, Tech. Rep. October (TU Delft, 2006).

[44] J. Preijde, *Solar Thermal Propulsion for Spacecraft*, Tech. Rep. (TU Delft, 2014).

[45] D. M. Pino, *Solar Concentrator Demonstrator for PocketQubes*, Tech. Rep. (TU Delft, 2016).

[46] D. M. Pino, B. Zandbergen, and O. Bergsma, *Solar Concentrator Demonstrator for PocketQubes,* EUCASS , 1 (2016).

[47] J. Bouwmeester, https://www.tudelft.nl/lr/delfi-space/delfi-program/, *Delfi program,* (2004).

[48] K. Anflo and R. Möllerberg, *Flight demonstration of new thruster and green propellant technology on the PRISMA satellite,* Acta Astronautica **65**, 1238 (2009).

[49] D. T. Schmuland, R. K. Masse, and C. G. Sota, *Hydrazine Propulsion Module for CubeSats,* (2011).

[50] NIST, https://webbook.nist.gov/cgi/cbook.cgi?ID=C7727379{&}Units=SI{&}Mask=1{#}Thermo-Gas, *Nitrogen,* (2018).

[51] K. Das, *Study of MEMS Design of a Solar Thermal Thruster*, Tech. Rep. (TU Delft, 2018).

[52] Z. S. Zhumaev and G. A. Shcheglov, *Operations dynamics analysis of solar thermal propulsion for CubeSats,* Advances in Space Research **64**, 815 (2019).

[53] G. Millis, *Design Factors for Applying Cryogen Storage and Delivery Technology to Solar Thermal Propulsion,* in *Space Technology and Applications International Forum* (1997).

[54] L. Engineering, https://www.lmnoeng.com/Flow/GasViscosity.php, *Gas Viscosity Calculator,* (2013).

[55] E. Edge, https://www.engineersedge.com/physics/water__density_viscosity_specific_weight_13146.htm, *Water - Density Viscosity Specific Weight,* (2019).

[56] R. R. Energy, http://www.redrok.com/concept.htm{#}emissivity, *Solar Absorption & Emissivity.* (2017).

[57] Thermocoupleinfo.com, https://www.thermocoupleinfo.com/thermocouple-accuracies.htm, *Thermocouple Accuracies,* (2011).

[58] B. Sensors, https://produktinfo.conrad.com/datenblaetter/500000-524999/502052-an-01-en-DRUCKTRANSMITTER_20_MA__0___16_BAR.pdf, *Operation manual,* (2015).

[59] F. Valente, *Development and verification of test set up for microthrusters testing*, Tech. Rep. (TU Delft, 2007).

[60] Brooks, *Profibus-DP Interface for use with Brooks ® Smart Mass Flow Meters,* (2008).

[61] The Engineering ToolBox, https://www.engineeringtoolbox.com/gas-density-d_158.html, *Gases - Densities,* (2003).

[62] L. S. Facts, https://www.lasersafetyfacts.com/4/, *Class 4 (IV) laser safety information,* (2019).

A

Python code for STP tool

```
"""
Model for STP v4
July 2019
A. Takken
"""

### import packages
import numpy as np
import matplotlib.pyplot as plt
from scipy.optimize import fsolve



### 1) feed system model
def feed(Mp,MMMat,propellant,pc,p_ltubing,p_lRAC,R_A,Tprop,B,rhot,sigmat,MMgas,c,j):

    MMprop = MMMat[propellant] #[kg/mol], propellant molar mass

    pfeed = pc + p_ltubing+p_lRAC #[Pa], propellant pressure
    pgasf = pfeed #[Pa], pressurant end pressure
    pgasi = B*pgasf #[Pa], pressurant start pressure

    Vp = Mp*R_A/MMprop*Tprop/pfeed #[m3], propellant volume
    Vg = Vp/(B-1) #[m3], pressurant volume
    Vt = Vp+Vg #[m3], tank volume

    Mg = pgasf*Vt/(R_A/MMgas*Tprop) #[kg], pressurant mass

    Rt = (Vt/(c*np.pi+4/3*np.pi))**(1/3) #[m], tank shell radius
    t = pgasi*Rt/sigmat*j #[m], thickness cylinder wall
    Lt = (Vt-4/3*np.pi*Rt**3)/(np.pi*Rt**2) #[m], tank cylinder length
    Vmat = np.pi*(Rt**2-(Rt-t)**2)*Lt+4/3*np.pi*(Rt**3-(Rt-(t/2))**3) #[m3], tank material
                                                                        volume
    Mshell = rhot*Vmat #[kg], tank shell mass

    K = 6.84*(Vt*1000)**(-0.2067) #[-], tank-to-shell ratio
    Mt = K*Mshell #[kg], tank mass
    Mtub = 0.20*Mt #[kg], tubing mass

    pRACi = pfeed-p_ltubing/2

    return Mt,MMprop,Mg,Mtub,pRACi


### 2) RAC model
def RAC(Dtub,Pin,alpha,m,n,Ltub,EmpMat,propellant,MMp,Tp0,pRACi,Rp,mdot,a,k_RAC,k_p,eps1,eps2
                                                                                    ):
```

```
Across = np.pi*(Dtub/2)**2                                  #[m2], tubing cross-sectional
                                                            area

Pinn = Pin*alpha/m/n                                        #[W], absorbed power per segment
                                                            (total of n segments and x channels)
qinn = Pinn/(Ltub/n)/Dtub                                   #[W/m2], absorbed flux per
                                                            segment (total of n segments and x
                                                            channels)

Hcrit0 =  (EmpMat[propellant][0][0]*(500.0/1000) + EmpMat[propellant][1][0]*(500.0/1000)
                                                            **2/2 + EmpMat[propellant][2][0]*(500.0/
                                                            1000)**3/3 + EmpMat[propellant][3][0]*(500
                                                            .0/1000)**4/4 - EmpMat[propellant][4][0]/(
                                                            500.0/1000) + EmpMat[propellant][5][0] -
                                                            EmpMat[propellant][6][0])/MMp*1000
                                                                  #[J/kg], enthalpy at first border
                                                            point
Hcrit1 = (EmpMat[propellant][0][1]*(2000.0/1000) + EmpMat[propellant][1][1]*(2000.0/1000)
                                                            **2/2 + EmpMat[propellant][2][1]*(2000.0/
                                                            1000)**3/3 + EmpMat[propellant][3][1]*(
                                                            2000.0/1000)**4/4 - EmpMat[propellant][4][
                                                            1]/(2000.0/1000) + EmpMat[propellant][5][1
                                                            ] - EmpMat[propellant][6][1])/MMp*1000
                                                                #[J/kg], enthalpy at second border
                                                            point

Xm,T0m,T1m,Tpm,T2m,T3m,cpm,Reym,p_ltubm = [],[],[],[],[],[],[],[],[]     #starting
                                                            matrices
Tp = Tp0                                                                  #[K], starting
                                                            propellant temperature
p_p = pRACi                                                               #[Pa], starting
                                                            propellant pressure
p_ltub = 0.0                                                              #[Pa], starting
                                                            tubing pressure losses
Econv = 0.0                                                               #[J/kg], starting
                                                             propellant energy gain

for j in range(1,n):

    if propellant == 0: #nitrogen
        if Tp < 500.0:
            i = 0
        elif Tp < 2000.0:
            i = 1
        else:
            i = 2
    if propellant == 1: #water
        if Tp < 500.0:
            i = 0
        elif Tp < 1700.0:
            i = 1
        else:
            i = 2
    if propellant == 2: #ammonia
        if Tp < 1400.0:
            i = 0
        else:
            i = 1
    if propellant == 3: #hydrogen
        if Tp < 1000.0:
            i = 0
        elif Tp < 2500.0:
            i = 1
        else:
            i = 2

    cp = (EmpMat[propellant][0][i] + EmpMat[propellant][1][i]*(Tp/1000) + EmpMat[
                                                            propellant][2][i]*(Tp/1000)**2 +
                                                            EmpMat[propellant][3][i]*(Tp/1000)**3
                                                            + EmpMat[propellant][4][i]/(Tp/1000)**
```

```
                                                    2)/MMp #[J/K/kg], heat coefficient
gamma = cp/(cp-Rp)                                                  #[-], heat
                                                    capacity ratio

rhop = (p_p-p_ltub)/(Rp*Tp)                                         #[kg/m3],
                                                    propellant density
v = mdot/m/rhop/Across                                              #[m/s],
                                                    propellant flow velocity
Pr = 4*gamma/(9*gamma-5)                                            #[-], Prandtl
                                                     number (assumed for gases)
mu = Pr*k_p/cp                                                      #[kg/m/s],
                                                    dynamic viscosity
halpha = a*rhop**0.8*v**0.8/Dtub**0.2*k_p*Pr**0.33/mu**0.8          #[W/m2/K],
                                                    coefficient of convective heat
                                                    transfer


T0 = 0.0
qcond1,qconv1 = 1,0
while abs(qcond1-qconv1) > 1e-6:

    T0 += abs(qcond1-qconv1)/100000.0
    qrad1 = eps1*sigma*(T0**4-T_RAC**4)
    qcond1 = qinn-qrad1
    T1 = T0-qcond1/k_RAC*D_RAC
    qconv1 = halpha*(T1-Tp)


T2 = 0.0
qconv2, qrad2 = 1,0
while abs(qconv2-qrad2) > 1e-6:

    T2 += abs(qconv2-qrad2)/100000.0
    qconv2 = halpha*(Tp-T2)
    T3 = T2-qconv2/k_RAC*D_RAC
    qrad2 = eps2*sigma*(T3**4-Tamb**4)


Pconv = (qconv1-qconv2)*Ltub/n*Dtub                                 #[W],
                                                    convective heat
Econv += Pconv/(mdot/m)                                             #[J/kg],
                                                    convective heat

if Econv < Hcrit0:
    i = 0
elif Econv < Hcrit1:
    i = 1
else:
    i = 2

func = lambda T : Econv - (EmpMat[propellant][0][i]*(T/1000) + EmpMat[propellant][1][
                                                    i]*(Tp/1000)**2/2 + EmpMat[propellant]
                                                    [2][i]*(Tp/1000)**3/3 + EmpMat[
                                                    propellant][3][i]*(Tp/1000)**4/4 -
                                                    EmpMat[propellant][4][i]/(Tp/1000) +
                                                    EmpMat[propellant][5][i] - EmpMat[
                                                    propellant][6][i])/MMp*1000 #[J/K/kg],
                                                     heat coefficient
func_initial = Tp0
Tp = fsolve(func,func_initial)[0]                                   #[K],
                                                    resulting propellant temperature after
                                                     nth element


Reynolds = rhop*v*Dtub/mu                                           #[-],
                                                    Reynolds number
if Reynolds < 2320:
    f = 64/Reynolds
elif Reynolds >= 2320 and Reynolds < 10^4:
    f = 0.316*(1/Reynolds)**(0.25)
else:
    f = 0.184*(1/Reynolds)**(0.2)
```

```
        p_ltub += f*(Ltub/n)/Dtub*1/2*rhop*v**2                                    #[Pa], tubing
                                                    pressure loss

        Xm.append(Ltub/n*j)
        T0m.append(T0)
        T1m.append(T1)
        Tpm.append(Tp)
        T2m.append(T2)
        T3m.append(T3)
        cpm.append(cp)
        Reym.append(Reynolds)
        p_ltubm.append(p_ltub)

    eta = Econv*mdot/Pin*100.0                                                     #[-], heat
                                                exchanger efficiency
    print("---")
    print(PropM[propellant])
    print("Final propellant temperature (Tp):","%.1f" % Tp,"[K]")
    print("Heat exchanger overal efficiency (eta):","%.1f" % eta,"%")
    print("Propellant pressure loss (P_ltub):","%.1f" % p_ltub,"[Pa]")

    plt.figure(1)
    plt.plot(Xm,T0m,label="T0")
    plt.plot(Xm,T1m,label="T1")
    plt.plot(Xm,Tpm,label="Tp")
    plt.plot(Xm,T2m,label="T2")
    plt.plot(Xm,T3m,label="T3")
    plt.xlabel("x [m]")
    plt.ylabel("T [K]")
    plt.legend()

    plt.figure(2)
    plt.plot(Xm,cpm)
    plt.xlabel("x [m]")
    plt.ylabel("cp [J/K/kg]")

    plt.figure(3)
    plt.plot(Xm,Reym)
    plt.xlabel("x [m]")
    plt.ylabel("Reynolds number [-]")

    plt.figure(4)
    plt.plot(Xm,p_ltubm)
    plt.xlabel("x [m]")
    plt.ylabel("delta P [Pa]")

    return p_ltub,eta,Tp,rhop,v,i


### 3) nozzle and performance tool
def nozzle(Tp,Rp,EmpMat,mdot,pc,pamb,propellant,i,MMp):

    cp = (EmpMat[propellant][0][i] + EmpMat[propellant][1][i]*(Tp/1000) + EmpMat[propellant][
                                                2][i]*(Tp/1000)**2 + EmpMat[propellant][3]
                                                [i]*(Tp/1000)**3 + EmpMat[propellant][4][i
                                                ]/(Tp/1000)**2)/MMp #[J/K/kg], heat
                                                coefficient

    gamma = cp/(cp-Rp)                                                             #[-], specific heat ratio
    Gamma = np.sqrt(gamma)*(2/(gamma+1))**((gamma+1)/(2*(gamma-1)))                #[-], Vandenkerckhove
                                                function

    At = mdot*np.sqrt(Rp*Tp)/Gamma/pc                                              #[m2], throat area
    Dt = np.sqrt(4*At)                                                             #[m], throat diameter

    pe = pamb                                                                      #[Pa], exit pressure (
                                                adapted nozzle)
    pstar = pc*(2/(gamma+1))**(gamma/(gamma-1))                                    #[Pa], critical pressure

    pratio = pe/pc                                                                 #[-], pressure ratio
```

```
    Aratio = Gamma/np.sqrt(2*gamma/(gamma-1)*pratio**(2/gamma)*(1-pratio**((gamma-1)/gamma)))
                                                    #[-], area ratio
    Ae = Aratio*At                                                  #[m2], exit area

    #Reynolds number calculation (https://www.lmnoeng.com/Flow/GasViscosity.php)
    Mt = 1
    Tt = (1+(gamma-1)/2*Mt**2)**(-1)*Tp

    if propellant != 1:                             #different calculation for water
        T0m = [540.99, 0, 527.67,528.93]
        Cm = [111, 0, 370, 72]
        mu0m = [0.01781e-3,0,0.00982e-3,0.00876e-3]
        T0 = T0m[propellant]                        #[deg Rankine], reference temperature
        C = Cm[propellant]                          #[deg Rankine], Sutherland's constant
        mu0 = mu0m[propellant]                      #[Pas], reference viscosity

        Ttrank = (Tt-273.15)*1.8000 + 491.67        #[deg Rankine], chamber temperature
        a = 0.555*T0+C                              #[deg Rankine], factor
        b = 0.555*Ttrank+C                          #[deg Rankine], factor
        mut = mu0*(a/b)*(Ttrank/T0)**(3/2)          #[Pa s], dynamic viscosity

    else: #https://www.engineersedge.com/physics/
                                                      water__density_viscosity_specific_weight_13146
                                                      .htm
        A = 2.414e-5                                #[K], factor
        B = 247.8                                   #[K], factor
        C = 140                                     #[K], factor
        mut = A*10^(B/(Tp-C))                       #[Pa s], dynamic viscosity

    Ret = 4*mdot/np.pi/Dt/mut                       #[-], throat Reynolds number

    if propellant != 3:
        a = (0.96-0.9275)/(0.011-0.0205)            #[-], factor (from TRP reader, page 194)
        b = 0.96-a*0.011                            #[-], factor (from TRP reader, page 194)
    else:
        a = (0.97-0.94)/(0.008-0.016)               #[-], factor (from TRP reader, page 194)
        b = 0.97-a*0.008                            #[-], factor (from TRP reader, page 194)

    Cd = a/Ret**(1/2)+b                             #[-], discharge coefficient

    #
    UL = np.sqrt(2*gamma/(gamma-1)*Rp*Tp)             #[m/s], limiting velocity
    Ue = UL*np.sqrt(1-(pe/pc)**((gamma-1)/gamma))     #[m/s], exhaust velocity
    Ueq = Ue + (pe-pamb)/mdot*Ae                      #[m/s], equivalent velocity

    F = mdot*Ueq                                      #[N], thrust
    Freal = Cd*mdot*Ueq                               #[N], real thrust
    Isp = Ueq/g0                                      #[s], specific impulse
    cstar = np.sqrt(Rp*Tp)/Gamma                      #[m/s], characteristic velocity

    ### output parameters
    if pe < pstar:
        flowc = "Yes"
    else:
        flowc = "No"

    print("Thrust (real):","%.1f" % (Freal*1000),"[mN]")
    print("Specific impulse:","%.1f" % Isp,"[s]")

    return F,Freal,Isp,cstar,flowc



###Constants
g0 =            9.81                    #[m/s2], gravitational acceleration Earth SL
R_A =           8.314                   #[J/K/mol], universal gas constant
PropM =         ["Nitrogen","Water",
                 "Ammonia","Hydrogen"]  #[-], investigated propellants
pamb0 =         1.01325e5               #[Pa], ambient pressure Earth SL

EmpMat = [[[28.98641,19.50583,35.51872],[1.853978,19.88705,1.128728],
```

```
            [-9.647459,-8.598535,-0.196103],[16.63537,1.369784,0.014662],
            [0.000117,0.527601,-4.553760],[-8.671914,-4.935202,-18.97091],
            [0.0,0.0,0.0]],[[-203.6060,30.09200,41.96426],[1523.290,6.832514,8.622053],
             [-3196.413,6.793435,-1.499780],[2474.455,-2.534480,0.098119],
             [3.855326,0.082139 ,-11.15764],[-256.5478,-250.8810,-272.1797],
             [-285.8304,-241.8264,-241.8264]],[[19.99563,52.02427],[49.77119,18.48801],[-15.
                                                    37599,-3.765128],
             [1.921168,0.248541],[0.189174,-12.45799],[-53.30667,-85.53895],
             [-45.89806,-45.89806]],[[33.066178,18.563083,43.413560],[-11.363417,12.257357,-4
                                                    .293079],
            [11.432816,-2.859786,1.272428],[-2.772874,0.268238,-0.096876],
            [-0.158558,1.977990,-20.533862],[-9.980797,-1.147438,-38.515158],
            [0.0,0.0,0.0]]]

MMMat = [28.0134e-3,18.0153e-3,17.0305e-3,2.01588e-3]    #[kg/mol], molar masses
k_pMat = [0.20,0.5918,0.507,0.1819]                      #[W/m/K], thermal conductivities

###Inputs & execution
#Feed system inputs
Mp =            0.500                   #[kg], propellant mass
propellant =    0                       #[-], 0 for nitrogen, 1 for water, 2 for ammonia, 3
                                            for hydrogen
pc =            2.0e5                   #[Pa], feed pressure
p_ltubing =     1.0*pc                  #[Pa], pressure losses from tank to RAC
p_lRAC =        0.3e5                   #[Pa], pressure losses in RAC
Tp =            273.15+25.0             #[K], propellant temperature
B =             4.0                     #[-], blow down ratio
rhot =          2.810e3                 #[kg/m3], tank density (aluminium 7075 T6)
sigmat =        480e6                   #[Pa], yield strength (aluminium 7075 T6)
MMgas =         4.003e-3                #[kg/mol], pressurant molar mass (helium)
c =             2.0                     #[-], length-to-radius ratio
j =             2.0                     #[-], safety factor

#Feed system execution
Mt,MMp,Mg,Mtub,pRACi = feed(Mp,MMMat,propellant,pc,p_ltubing,p_lRAC,R_A,Tp,B,rhot,sigmat,
                                            MMgas,c,j)

#RAC inputs
Pin = 1000.0                            #[W], incoming irradiance power
sigma = 5.670e-8                        #[W/m2/K4], Stefan-Boltzmann constant
a = 0.023                               #[-], constant for convection
Tamb = 298.15                           #[K], ambient temperature

alpha = 0.90                            #[-], absorption RAC inner wall
eps1 = 0.80                             #[-], emissivity RAC inner wall
eps2 = 0.10                             #[-], emissivity RAC outer wall
k_RAC = 401                             #[W/m/K], thermal conductivity RAC material
D_RAC = 0.005                           #[m], RAC thickness (both front- and backside)
T_RAC = 298.15                          #[K], RAC starting temperature
Ltub = 0.10                             #[m], tubing length
Dtub = 0.002                            #[m], tubing diameter
m = 8                                   #[-], number of channels

mdot = 300.0e-6                         #[kg/s], total mass flow
k_p = k_pMat[propellant]                #[W/m/K], thermal conductivity propellant
Tp0 = 298.15                            #[K], starting propellant temperature

n = 100                                 #[-], number of elements
Rp = R_A/MMMat[propellant]              #[J/K/kg], specific gas constant

#RAC execution
p_ltub,eta,Tp,rhop,v,i = RAC(Dtub,Pin,alpha,m,n,Ltub,EmpMat,propellant,MMp,Tp0,pRACi,Rp,mdot,
                                            a,k_RAC,k_p,eps1,eps2)

#Nozzle & performance inputs
pamb0 = 1.01325e5                       #[Pa], SL pressure
pamb = 1.00*pamb0                       #[Pa], ambient pressure

#Nozzle & performance execution
F,Freal,Isp,cstar,flowc = nozzle(Tp,Rp,EmpMat,mdot,pc,pamb,propellant,i,MMp)
```

B

Test plan

In this chapter, the test plan is presented which is used for the test of the thruster and the heat source. It is started off by an introduction, stating the background of the experiment. It is followed by a description of the objectives of the experiments, followed by the design of the tests. After that, the required tools and materials are described. Finally, safety regulations are given. The test plan lay-out is based on the website https://tinyurl.com/gwkqx6h.

B.1. Introduction

As part of the thesis at the faculty of AE at DUT, research is conducted towards the subject of STP. STP is a satellite propulsion concept wherein thrust is generated by the direct heating of a propellant by solar radiation. STP has been proven a suitable propulsion method for certain types of mission because of its higher efficiency (specific impulse) than conventional thermal rockets while having superior thrust levels with respect to electric thrusters. It has been extensively treated in theoretical studies but has rarely been tested in laboratories and has never flown in space. Thus, the assignment for the thesis is to prove that STP can be competitive to other propulsion subsystems. To make this proof, the focus will be on showing that the specific impulse can be raised to a competitive level, in the range of 100.0 s, at a thrust level of 100 mN. More information can be found in the attached Project plan document (AD-1).

For the thesis, an STP microthruster will be designed, built and tested. This microthruster will consist of an RAC, which will be illuminated during the test. In the RAC's walls, propellant (most likely gaseous nitrogen) will flow and be heated by the radiation. The propellant will then be expelled through a nozzle in order to generate thrust. See Figure B.1 for a schematic overview of the STP concept [4]. Please note that no concentrator will be used in this thesis.

It is required to have a suitable heat source that delivers substantial power in a controlled manner. The laser setup at the faculty of 3mE (DUT) was identified as a heat source that meets these requirements (see Section 4.1). The power output can be regulated from 50 W to 8000 W in steps of 1 W.

This document will describe the test plan, in which the setup is explained, the relevance is given and the protocol is described. The added documents are:

- [AD-1] A. Takken (2019) [AT-PRP-DOC-5.0] AE4010 Project plan [2]

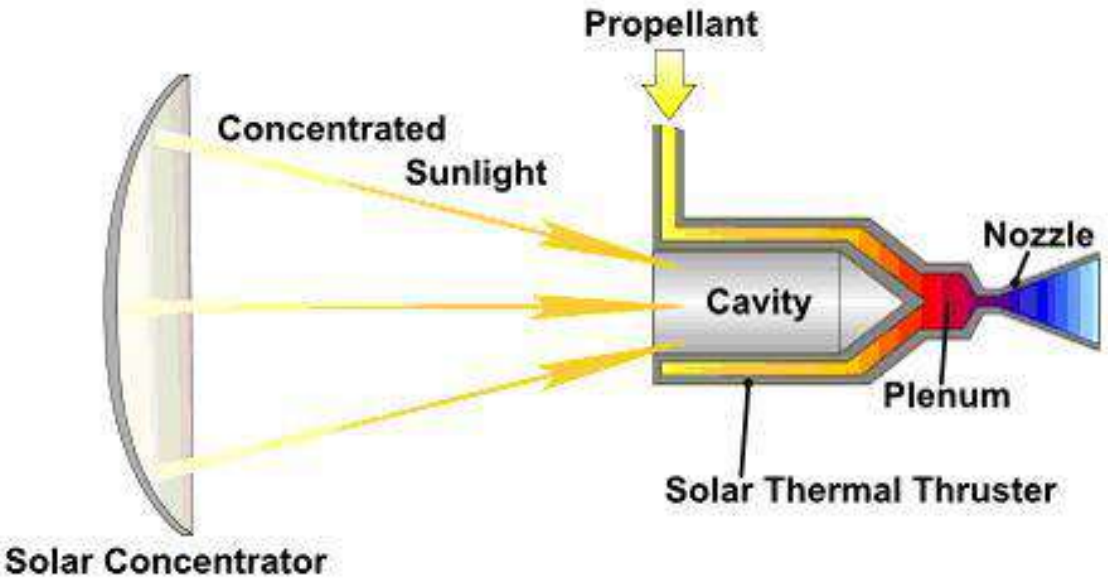

Figure B.1: Schematic overview of the STP concept [4].

- [AD-2] F. Valente (2010) [FV-TSB-DOC-1.0] Thrust bench TB-1.1 [59]

B.2. Experiment objectives

The goal of the thesis is (see also AD-1) to demonstrate the feasibility of solar thermal propulsion. This will be done by designing, manufacturing and testing an STP engine for nanosatellite applications. There will be two tests with its corresponding objectives:

1. No heating test. The thruster setup will be placed under the laser equipment. The laser will be turned off, but propellant will run through the engine in this experiment. Objective is to assess the performance without heating by measuring the thrust and mass flow. This test can also be done at another location because no heat source is needed.
2. Full engine test. This experiment will be completely the same as the dry test, but there will be a propellant flow. Objective is to measure the performance (especially thrust) and validate the performance tool of the thruster and assess the feasibility of the thruster. If time allows, power input and propellant mass flow will be adjusted during runs to study its effects.

B.3. Experiment design

As can be seen in the previous section, the test will be done in two parts. Before these two experiments commence, the laser will first be calibrated using the power meter available in the laser facility. For this, the power meter will be placed at the same distance as the RAC will be during both tests. The laser input and resulting power meter output will be saved, while the laser input will slowly be ramped up from <TBD> W to <TBD> W. After the data is saved, the laser will be turned off and the meter (after cooling down) will be removed.

Then the experiments will start. In both experiments, the thruster system will be fully setup. Please refer to Section B.4 for all necessary equipment. The engine (nozzle, RAC and tubing) will be mounted in the thrust bench (see AD-2 for more information). The thrust bench will be placed in the laser setup, so that the laser will be pointed towards the RAC. The distance between RAC and laser will be <TBD>

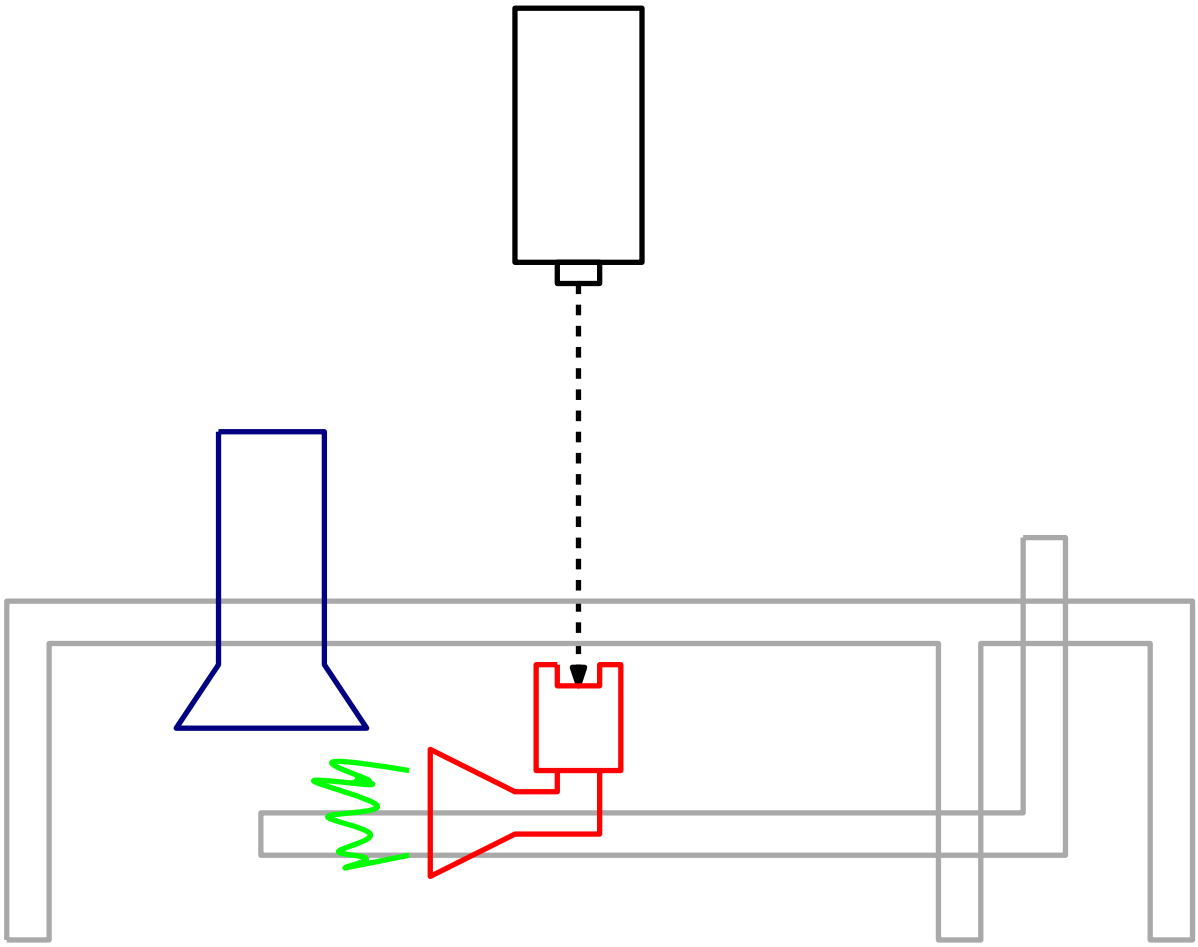

Figure B.2: Sketch showing the test setup.

m and will mainly depend on the laser beam width. Furthermore, care should be taken that the nozzle outlet is not pointed towards any user and is close to the suction fan, as hot flow will be ejected in the second experiment. See Figure B.2 for a sketch showing the test setup. The engine is outlined in red with green propellant flow. It receives irradiation from the laser optical head and is mounted within the (gray) thrust bench. The suction fan is outlined in blue.

The thermocouples, pressure sensors, load sensor and propellant mass flow sensor will be connected (via NI devices) to a laptop and grid if needed. LabVIEW (see Subsection 4.2.2) will be run from this laptop to acquire data from the sensors. If necessary, the laptop and NI devices need to be shielded from the radiation. The LabVIEW script on the laptop will be run to ensure that data is acquired. The position of the thrust bench under the laser is verified.

Then, the first experiment will commence by starting the script and turning on the laser at the lowest power setting (<TBD> W). When steady state is reached (the temperature in the engine does not change anymore), the laser power will be increased. This will be done in steps of <TBD> W until the final power of <TBD> W is reached. It is believed that about <TBD> s are necessary each step, so the total time is (conservatively) about <TBD> minutes. When the final power is reached, the laser will be shut down and the engine will be given time to cool down to room temperature.

After that, the second experiment will start. It will largely be the same as the first experiment, but now the propellant valve will be open. First, the laser will be turned off while the propellant valve will deliver a flow of <TBD> bar. Data will be acquired, after which various combinations of mass flow and laser power will be made and observed. Afterwards, the valve will be closed, the laser shut down

and the engine will be allowed to cool down. A total time of <TBD> minutes is expected. Finally, the engine setup will be disassembled and cleaned up.

Because experiments are prone to unforeseen events, it would be wise to allocate two time slots for the testing, with a few weeks in between. This way it is ensured that any faults made on the first day can be corrected in the second one. Please note that no vacuum environment is present during the experiments, because it is deemed too complex to transport a vacuum chamber or oven to the welding facility.

B.4. Required materials

For the test, the equipment required is listed in Table B.1.

Equipment number	Name	Function	Reference
1	Thruster nozzle	Part of the STP thruster	Section 2.1
2	Thruster RAC	Part of the STP thruster	Section 2.1
3	Thruster tubing	Part of the STP thruster	Section 2.1
4	Propellant tank	Contains gaseous nitrogen as propellant, delivered by the Gassenteam	Section 3.1
5	Mass flow sensor & regulator	To regulate and measure the mass flow and propellant inlet pressure, delivered by the Gassenteam	Subsection 4.2.6
6	Thrust bench	To hold the STP thruster, developed in 2010 by F. Valente	AD-2
7	Load sensor	To measure the thrust, connected to the thrust bench	Subsection 4.2.5
8	Thermocouples (6)	To measure the temperature, RS PRO Type N	Subsection 4.2.3
9	Pressure sensors (2)	To measure the pressure	Subsection 4.2.4
10	Laptop & charger	To collect the data from the sensors (via LABview)	Subsection 4.2.2
11	Plug box	To connect the pressure sensors and laptop to the power grid	-
12	NI temperature devices (2)	Type NI 9211, to connect the thermocouples to the laptop	Subsection 4.2.3
13	NI pressure device	To connect the pressure sensor to the laptop	Subsection 4.2.4
14	NI voltage NI	To connect the load sensor to the laptop	Subsection 4.2.5
15	Heat shield	To shield the sensors and other equipment from excessive heat from the heat source	-
16	Barometer	To measure the ambient pressure	-
17	Temperature sensor	To measure the ambient temperature	-
18	Heat source (including suction fan)	To heat up the propellant in the thruster RAC via radiation	Section 4.1
19	Power meter	To measure the output radiation from the heat source	Subsection 4.2.7

Table B.1: Required equipment during experiments.

All equipment will be brought in by the thesis student, except for the last two pieces. These two

are already present at the laser facility.

B.5. Safety regulations

The laser setup is a class 4 laser, which is the highest (most severe) class for laser equipment [62]. Extreme care should be taken that nothing interferes with the laser beam. Protective glasses and safety footwear should be worn. The door is equipped with an interlock system which shuts down the laser when the door is opened.